

1 Review on “Inputs and processes affecting the distribution of particulate iron in the North
2 Atlantic along the GEOVIDE (GEOTRACES GA01) section” by Gourain et al.
3 The manuscript has improved much! I agree with the scientific findings and suggestions
4 made, but still the language is sometimes hard to follow and paragraphs are not always, but
5 sometimes very long. All this makes it to a real challenge to read the manuscript.
6
7

8 Dear Dr Schlosser,
9 We shortened some of the paragraphs to make it more readable as suggested. You will also
10 find our detailed answers to the specific points your raised below. We also joined the
11 manuscript with track change.
12 We truly hope that you will now find this manuscript suitable for publication.
13 Kind regards,
14 Arthur Gourain, on behalf of all coauthors.
15
16
17
18

19 From the scientific part, I have just some minor points, listed below
20 Line 32: Insert “thermohaline overturning circulation.” Done.

21
22 Line 131: I do not know what the Berger citation has to do with your results. I would remove
23 the Berger et al. citation! We rephrase this sentence: “...while the other half was archived at -
24 20 °C for SEM analyses or acid leaching of “labile” metals following Berger et al. (2008) method (to be
25 published separately).” Line 132.
26

27 Line 210: Include “Close to the sea floor...” Done.

28
29 Line 318: Replace (PMF, factor 3 = 4.1%) Done.

30
31 Line 319ff: Replace “, but its contribution is most likely obscured...” Done.

32
33 Line 321ff: The reasoning is plausible, but please shorten this paragraph, it is too long. You
34 can distill the message down to a couple sentences. We shortened the paragraph. From line
35 322 to line 335.
36

37 Line 388: Replace “in” by “to the Atlantic Ocean.” Done.
38

39 Line 401-409: I do not follow the reasoning! PP is high because of high DFe and elevated
40 primary productivity, which subsequently reduced DFe by biological utilization. First you
41 need to show that DFe concentrations are elevated. Then use Chl a to show that the
42 production is elevated, and then you may argue that the high PFe with a high PFe/Pal ratio
43 comes from elevated productivity. Values of DFe and Chl-a have been added to the
44 sentence. Line 399ff.
45

46 Line 410ff: Shorten the paragraph, you say a lot without saying something useful. We kept
47 this paragraph as it was. In this paragraph, we discuss the dispersion of the shelf signal for the
48 first and only time. We think it is important to keep it as it was.
49

50 Line 446ff: This paragraph is out of context. Also the next one, which I suppose was written
51 to sum up the results. But somehow it doesn't, maybe better to create another section.

52 [We deleted this paragraph.](#)

53
54 Line 466ff: What is new, that has not been said earlier. Nepheloid layers have been already
55 introduced! [The introductory paragraph is saying for the first time, the importance of](#)
56 [BNLs along GEOVIDE and their differences between each other. We think keeping this](#)
57 [paragraph here is important.](#)

58
59 Line 490ff: You could also use DFe and DMn as a tracer. What are these elements showing!
60 [DFe and DMn were not showing any elevated concentration above the ridge.](#)

61
62 Line 527ff: This is speculative! [From your previous comments, we modify the](#)
63 [paragraph Line 399ff in order to demonstrate this statement.](#)

64

65

66

67

68

69

70

71

72

73

74

75

76

77

78

79

80

81 **Inputs and processes affecting the distribution of particulate**
82 **iron in the North Atlantic along the GEOVIDE (GEOTRACES**
83 **GA01) section**

84
85

86 Arthur Gourain^{1,2}, H el ene Planquette¹, Marie Cheize^{1,3}, Nolwenn Lemaitre^{1,4}, Jan-Lukas
87 Menzel Barraqueta^{5,6}, Rachel Shelley^{1,7}, Pascale Lherminier⁸ and G eraldine Sarthou¹

88

89 1-UMR 6539/LEMAR/IUEM, CNRS, UBO, IRD, Ifremer, Technop ole Brest Iroise, Place Nicolas Copernic,
90 29280 Plouzan e, France

91 2- now at Ocean Sciences Department, School of Environmental Sciences, University of Liverpool, Liverpool,
92 L69 3GP, United Kingdom

93 3- now at Ifremer, Centre de Brest, G eosciences Marines, Laboratoire des Cycles G eochimiques (LCG), 29280
94 Plouzan e, France

95 4- now at Department of Earth Sciences, Institute of Geochemistry and Petrology, ETH-Z urich, Z urich,
96 Switzerland

97 5- GEOMAR, Helmholtz Centre for Ocean Research Kiel, Wischhofstra e 1-3, 24148 Kiel, Germany

98 6- now at Department of Earth Sciences, Stellenbosch University, Stellenbosch, 7600, South Africa

99 7- now at Earth, Ocean and Atmospheric Science, Florida State University, Tallahassee, Florida, 32310, USA

100 8- Ifremer, Univ. Brest, CNRS, IRD, Laboratoire d'Oc eanographie Physique et Spatiale (LOPS), IUEM, F-
101 29280, Plouzan e, France

102

103 *Correspondence to: helene.planquette@univ-brest.fr*

104

105 **Abstract**

106 The aim of the GEOVIDE cruise (May-June 2014, R/V *Pourquoi Pas?*) was to provide a better understanding of
107 trace metal biogeochemical cycles in the North Atlantic Ocean. As marine particles play a key role in the global
108 biogeochemical cycle of trace elements in the ocean, we discuss the distribution of particulate iron (PFe), in
109 relation to the distribution of particulate aluminium (PAI), manganese (PMn) and phosphorus (PP). Overall, 32
110 full vertical profiles were collected for trace metal analyses, representing more than 500 samples. This resolution
111 provides a solid basis for assessing concentration distributions, elemental ratios, size-fractionation, and adsorptive
112 scavenging processes in key areas of the thermohaline overturning circulation. Total particulate iron
113 concentrations ranged from as low as 9 pmol L⁻¹ in surface waters of the Labrador Sea to 304 nmol L⁻¹ near the
114 Iberian margin, while median PFe concentrations of 1.15 nmol L⁻¹ were measured over the sub-euphotic ocean
115 interior.

116 Within the Iberian Abyssal Plain, the ratio of PFe to PAI was identical to the continental crust molar ratio (0.21
117 mol mol⁻¹), indicating the important influence of crustal particles in the water column. Overall, the lithogenic

118 component explained more than 87% of PFe variance along the section. Within the Irminger and Labrador basins,
119 the formation of biogenic particles led to an increase of the PFe/PAI ratio (up to 0.64 mol mol⁻¹) compared to the
120 continental crust ratio. Continental margins provide high quantities of particulate trace elements (up to 10 nmol
121 L⁻¹ of PFe) to the open ocean. For example, horizontal advection of PFe was visible more than 250 km away from
122 the Iberian margin. Additionally, several benthic nepheloid layers were observed more than 200 m above the
123 seafloor along the transect, especially in the Icelandic, Irminger and Labrador basins, suspending particles with
124 high PFe content of up to 89 nmol L⁻¹.

125

126 **1. Introduction**

127 Particles play a key role in the ocean where they drive the residence time of most elements (Jeandel and Oelkers,
128 2015), and strongly influence the global biogeochemistry of macro- and micro-nutrients including iron (Milne et
129 al., 2017). In the surface ocean, biological activity produces biogenic suspended matter through planktonic
130 organisms, while atmospheric deposition (Baker et al., 2013; Jickells et al., 2005), riverine discharge (Aguilar-
131 Islas et al., 2013; Berger et al., 2008; Ussher et al., 2004) or ice-melting (Hawkings et al., 2014; Lannuzel et al.,
132 2011, 2014) deliver mostly lithogenic derived particles to surface waters. These particulate inputs are highly
133 variable, both spatially and seasonally, in the world's oceans. At depth, benthic and shelf sediment resuspension
134 (e.g. Aguilar-Islas et al., 2013; Cullen et al., 2009; Elrod et al., 2004; Fitzwater et al., 2000; Hwang et al., 2010;
135 Lam et al., 2015; Lam and Bishop, 2008; McCave and Hall, 2002), and hydrothermal activity (Elderfield and
136 Schultz, 1996; Lam et al., 2012; Tagliabue et al., 2010, 2017; Trefry et al., 1985), provides important amounts of
137 particles to the water column. Moreover, authigenic particles can be produced *in-situ* by aggregation of colloids
138 (Bergquist et al., 2007) or oxidation processes (Bishop and Fleisher, 1987; Collier and Edmond, 1984). Thus,
139 oceanic particles result from a complex combination of these different sources and processes (Lam et al., 2015).
140 In the upper water column, the total iron pool is dominated by marine particles (Radic et al., 2011) which strongly
141 interact with the dissolved pool (e.g. Ellwood et al., 2014). Indeed, dissolved iron can be scavenged onto particles
142 (Gerringa et al., 2015; Rijkenberg et al., 2014), incorporated into biogenic particles (Berger et al., 2008) or
143 produced by remineralisation of particles (Dehairs et al., 2008; Sarthou et al., 2008). Interestingly, the concept of
144 "reversible scavenging" (i.e. release at depth of dissolved iron previously scavenged onto particles) has been
145 advocated recently (Dutay et al., 2015; Jeandel and Oelkers, 2015; Labatut et al., 2014), while other studies reveal
146 distinct dissolution processes of inorganic particulate iron (e.g. Oelkers et al., 2012; Cheize et al., 2018). Slow
147 dissolution of particulate iron at margins has also been evoked as a continuous fertilizer of primary production
148 and should be considered as a source of dissolved iron (e.g. Jeandel et al., 2011; Jeandel and Oelkers, 2015; Lam
149 and Bishop, 2008). Within or below the mixed layer, the rates of regeneration processes can also impact the
150 bioavailable pool of iron, among other trace metals (e.g. Ellwood et al., 2014; Nuester et al., 2014). However, the
151 rates of these processes are not yet fully constrained. The study of particulate iron is thus essential to better
152 constrain its marine biogeochemical cycle. Interest has grown in this subject over the last 10 years, in particular
153 (e.g. Bishop and Biscaye, 1982; Collier and Edmond, 1984; Frew et al., 2006; Lam et al., 2012; Milne et al., 2017;
154 Planquette et al., 2011, 2013; Sherrell et al., 1998) and, to our knowledge, only two studies have been performed
155 on an ocean-wide scale: the GA03 GEOTRACES North Atlantic Zonal Transect (Lam et al., 2015; Ohnemus and
156 Lam, 2015) and the GP16 GEOTRACES Pacific Transect (Lam et al., 2017; Lee et al., 2017).

157 Within this global context, this paper presents the particulate iron distribution of the North Atlantic Ocean, along
158 the GEOTRACES GA01 section (GEOVIDE), and discusses the various sources and processes affecting
159 particulate iron (PFe) distribution, using particulate aluminium (PAI), phosphorus (PP) or manganese (PMn)
160 distributions to support our conclusions.
161

162 **2. Methods**

163 *2.1. Study area*

164 Particulate samples were collected at 32 stations during the GEOVIDE (GEOTRACES GA01 section) cruise
165 between May and June 2014 aboard the R/V *Pourquoi Pas?* in the North Atlantic Ocean (Sarthou et al., 2018).
166 The sampling spanned several biogeochemical provinces (Figure 1), starting over the Iberian margin (IM, Stations
167 2, 4 and 1), and proceeding to the Iberian Abyssal Plain (IAP, Stations 11 to 17), the Western European Basin
168 (WEB, Station 19 to Station 29) and the Icelandic Basin (IcB, Stations 32 to 36). Then, samples were collected
169 above the Reykjanes Ridge (RR, Station 38), in the Irminger Basin (IrB, Stations 40 to 60), close to the Greenland
170 shelf (GS, Stations 53, 56 and 61), the Labrador Basin (LB, Stations 63 to 77) and finally close the Newfoundland
171 shelf (NS, Station 78) (Figure 1). The North Atlantic is characterized by a complex circulation (briefly described
172 in section 3.1 and in detail by Zunino et al. (2017) and García-Ibáñez et al. (2015)) and is one of the most
173 productive regions of the global ocean (Martin et al., 1993; Sanders et al., 2014).
174

175

176 *2.2. Sampling*

177 Samples were collected using the French GEOTRACES clean rosette, equipped with twenty-two 12 L GO-FLO
178 bottles (two bottles were leaking and were not deployed during the cruise). GO-FLO bottles (General Oceanic's)
179 were initially cleaned in the home laboratory (LEMAR) following the GEOTRACES procedures (Cutter and
180 Bruland, 2012). The rosette was deployed on a 14 mm Kevlar cable with a dedicated, custom-designed clean
181 winch. Immediately after recovery, the GO-FLO bottles were individually covered at each end with plastic bags
182 to minimize contamination. Bottles were then transferred into a clean container (class-100) for sampling. On each
183 cast, nutrient and/or salinity samples were taken to check potential leakage of the GO-FLO bottles.

184 Filters were cleaned following the GEOTRACES protocols (<http://www.geotraces.org/images/Cookbook.pdf>)
185 and kept in acid-cleaned 1 L LDPE bottles (Nalgene) filled with ultrapure water (Milli-Q, resistivity of 18.2 M Ω
186 cm) until use. All filters were 25 mm diameter in order to optimize the signal over the filter blank, except at the
187 surface depth where 47 mm diameter filters were used. The filters were mounted on acid-cleaned polysulfone
188 filter holders (NalgeneTM). Prior to filtration, the GO-FLO bottles were shaken three times, as recommended in
189 the GEOTRACES cookbook to avoid settling of particles in the lower part of the bottle. GO-FLO bottles were
190 pressurized to < 8 psi with 0.2 μ m filtered nitrogen gas (N₂, Air Liquide). Seawater was then filtered directly
191 through paired filters (Pall Gelman SuporTM 0.45 μ m polyetersulfone, and Millipore mixed ester cellulose MF 5
192 μ m) mounted in Swinnex polypropylene filter holders (Millipore), following Planquette and Sherrell (2012) inside
193 the clean container. Filtration was operated until the bottle was empty or until the filter clogged; the volume
194 filtered ranged from 2 L for surface samples to 11 L within the water column. After filtration, filter holders were
195 disconnected from the GO-FLO bottles and a gentle vacuum was applied using a syringe in order to remove any

196 residual water under a laminar flow hood. Filters were then removed from the filter holders with plastic tweezers
197 (which were rinsed with Milli-Q between samples). Most of the remaining seawater was removed via ‘sipping’
198 by capillary action, when placing the non-sampled side of the filter onto a clean 47 mm supor filter. Each filter
199 pair was then placed in an acid-cleaned polystyrene PetriSlide (Millipore), double bagged, and finally stored at -
200 20 °C until analysis at LEMAR. Between casts, filter holders were thoroughly rinsed with Milli-Q, placed in an
201 acid bath (5% Trace metal grade HCl) for 24 hours, then rinsed with Milli-Q.

202 At each station, process blanks were collected as follows: 2 L of a deep (1000 m) and a shallow (40 m) seawater
203 sample were first filtered through a 0.2 µm pore size capsule filter (Pall Gelman Acropak 200) mounted on to the
204 outlet of the GO-FLO bottle before passing through the particle sampling filter, which was attached directly to
205 the swinnex filter holder.

206

207

207 *2.3. Analytical methods*

208 In the home laboratory, sample handling was performed inside a clean room (Class 100). All solutions were
209 prepared using ultrapure water (Milli-Q) and all plasticware had been acid-cleaned before use. Frozen filters,
210 collected within the mixed layer or within nepheloid layers, were first cut in half using a ceramic blade: one filter
211 half was dedicated to total digestion (see below), while the other half was archived at -20 °C for SEM analyses or
212 acid leaching of “labile” metals following (Berger et al., 2008); method (to be published separately).

213 Filters were digested following the method described in Planquette and Sherrell (2012). Filters were placed on
214 the inner wall of acid-clean 15 mL PFA vials (Savillex™), and 2 mL of a solution containing 2.9 mol L⁻¹
215 hydrofluoric acid (HF, suprapur grade, Merck) and 8 mol L⁻¹ nitric acid (HNO₃, Ultrapur grade, Merck) was added
216 to each vial. Vials were then closed and refluxed at 130 °C on a hot plate for 4 hours, after which the filters were
217 removed. After cooling, the digest solution was evaporated at 110 °C to near dryness. Then, 400 µL of
218 concentrated HNO₃ (Ultrapur grade, Merck) was added, and the solution was re-evaporated at 110 °C. Finally,
219 the obtained residue was dissolved with 3 mL of 0.8 mol L⁻¹ HNO₃ (Ultrapure grade, Merck). This archived
220 solution was transferred to an acid cleaned 15 mL polypropylene centrifuge tube (Corning®) and stored at 4 °C
221 until analyses.

222 All analyses were performed on a sector field inductively coupled plasma mass spectrometer (SF-ICP-MS
223 Element 2, Thermo-Fisher Scientific). Samples were diluted by a factor of 7 on the day of analysis in acid-washed
224 13 mm (outer diameter) rounded bottom, polypropylene centrifuge tubes (VWR) with 0.8 mol L⁻¹ HNO₃ (Ultrapur
225 grade, Merck) spiked with 1µg L⁻¹ of indium (¹¹⁵In) solution in order to monitor the instrument drift. Samples
226 were introduced with a PFA-ST nebulizer connected to a quartz cyclonic spray chamber (Elemental Scientific
227 Incorporated, Omaha, NE) via a modified SC-Fast introduction system consisting of an SC-2 autosampler, a six-
228 port valve and a vacuum-rinsing pump. The autosampler was contained under a HEPA filtered unit (Elemental
229 Scientific). Two 6-point, matrix-matched multi-element standard curves with concentrations bracketing the range
230 of the samples were run at the beginning, the middle and the end of each analytical run. Analytical replicates were
231 made every 10 samples, while accuracy was determined by performing digestions of the certified reference
232 material BCR-414 (plankton, Community Bureau of Reference, Commission of the European Communities),
233 PACS-3 and MESS-4 (marine sediments, National Research Council Canada), following the same protocol used
234 for the samples. Recoveries were typically within 10% of the certified values (and within the error of the data,
235 taken from replicate measurements, Table 1). Once all data were normalized to an ¹¹⁵In internal standard and

236 quantified using an external standard curve, the dilution factor of the total digestion was accounted for. The
237 elemental concentrations were obtained per filter (pmol/filter) and were then process blank-corrected. Finally,
238 pmol/filter values were divided by the volume of water filtered through stacked filters.
239 Total concentrations (sum of small size fraction (0.45-5 µm) and large (>5 µm) size fraction) of particulate trace
240 elements are reported in Table S1.

241

242 2.4. Positive matrix factorisation

243 Positive Matrix Factorisation (PMF) was run to characterise the main factors influencing the particulate trace
244 element variance along the GEOVIDE section. In addition to PFe, PAI, PMn, and PP, nine additional elements
245 were included in the PMF: yttrium (Y), barium (Ba), lead (Pb), thorium (Th), titanium (Ti), vanadium (V), cobalt
246 (Co), copper (Cu) and zinc (Zn). The PMF was conducted on samples where all elements were above their
247 detection limits; after selection, 445 of the 549 existing data points were used. Analyses were performed using
248 the PMF software, EPA PMF 5.0, developed by the USA Environmental Protection Agency (EPA). Three to six
249 factor models were run on the data. The configuration that provided the lowest error estimation (i.e. was the most
250 reliable) was the four factor model. To ensure stability, this model was run 100 times. After displacement, error
251 estimation and bootstrap error estimation, the model was recognised as stable.

252

253 2.5. Derived and ancillary parameters

254 To investigate the proportion of lithogenic iron within the bulk particulate iron, we used the Upper Continental
255 Crust (UCC) Fe/Al molar ratio (0.21) of Taylor and McLennan (1995) to calculate the lithogenic components of
256 particles (%PFe_{litho}) following Eq. (1):

257

$$258 \quad \%PFe_{litho} = 100 * \left(\frac{PAI}{PFe} \right)_{sample} * \left(\frac{PFe}{PAI} \right)_{UCCratio} \quad (1)$$

259

260 The non-lithogenic PFe is obtained using Eq. (2):

261

$$262 \quad \%PFenon_{litho} = 100 - \%PFe_{litho} \quad (2)$$

263

264 Note that while the %PFe_{litho} and %PFe_{non-litho} proxies are interesting tools to evaluate the importance of lithogenic
265 and non-lithogenic (either biogenic or authigenic) fraction, they have to be used carefully, as the spatial and
266 temporal variation of the lithogenic component ratios may involve uncertainties of the estimated fraction value.

267 In addition to PAI, PMn can be used as a tracer of inputs from shelf resuspension (Lam and Bishop, 2008), using
268 a percentage of sedimentary inputs “%bulk sediment inputs” estimated according to the following equation:

$$269 \quad \%bulksedimentPMn = 100 * \left(\frac{PAI}{PMn} \right)_{sample} * \left(\frac{PMn}{PAI} \right)_{UCCratio} \quad (3)$$

270 with PAI/PMn being the ratio from the GEOVIDE samples and the PMn/PAI being the UCC value (0.0034; Taylor
271 and McLennan, 1995).

272 This proxy can be a good indicator of sediment resuspension. We assume that particles newly resuspended in the
273 water column will have the same PMn/PAI ratio as the UCC ratio, leading to a “%bulk sediment Mn” of 100%.
274 This proxy assumes homogeneity of the sediment PMn/PAI ratio throughout the GEOVIDE section. However,
275 this may not be the case at every station. In consequence, this proxy should only be used to identify new benthic
276 resuspension at specific locations; inter-comparison between several locations may not be appropriate. When a
277 sample presents a “%bulk sediment Mn” greater than 100%, we have assigned a maximum value of 100%. As the
278 Mn cycle can also be influenced by biotic uptake (e.g. Peers and Price, 2004; Sunda and Huntsman, 1983), this
279 proxy is only used at depths where biologic activity was negligible (i.e. below 150m depth).

280 Potential temperature (θ°), salinity (S), and transmissometry data were retrieved from the CTD sensors (CTD
281 SBE911 equipped with a SBE43).

282

283

284 3. Results

285 3.1. Hydrography setting

286 Here, we briefly describe the hydrography encountered during the GEOVIDE section (Figure 2) as a thorough
287 description is available in García-Ibáñez et al. (2015). At the start of the section, the warm and salty Mediterranean
288 Water (MW, $S = 36.50$, $\theta^\circ = 11.7$ °C) was sampled between 600 and 1700 m in the Iberian Abyssal Plain (IAP).
289 MW resulted from the mixing between the Mediterranean Overflow Water (MOW) plume coming from the
290 Mediterranean Sea and local waters. Surface water above the Iberian Shelf was characterised by low salinity ($S =$
291 34.95) at station 2 and 4 compared to surrounding water masses. Close to the sea floor of the Iberian Abyssal
292 Basin, the North East Atlantic Deep Water (NEADW, $S = 34.89$, $\theta^\circ = 2.0$ °C) spread northward. The North
293 Atlantic Central Water (NACW, $S > 35.60$, $\theta^\circ > 12.3$ °C) was the warmest water mass of the transect and was
294 observed in the subsurface layer of the Western European Basin and Iberian Abyssal Plain. An old Labrador Sea
295 Water (LSW, $S = 34.87$, $\theta^\circ = 3.0$ °C) flowed inside the Western European and Icelandic Basins, between 1000
296 and 2500m depth.

297 In the Icelandic Basin, below the old LSW, the Iceland-Scotland Overflow Water (ISOW, $S = 34.98$, $\theta^\circ = 2.6$ °C)
298 spread along the Reykjanes Ridge slope. This cold water, originating from the Arctic, led to the formation of
299 NEADW after mixing with surrounding waters. North Atlantic hydrography was impacted by the northward
300 flowing of the North Atlantic Current (NAC), which carried warm and salty waters from the subtropical area. Due
301 to air-sea interactions and mixing with surrounding water, the NACW is cooled and freshened in the subpolar
302 gyre and is transformed in Subpolar Mode Water (SPMW). The formation of SPMW inside the Icelandic and
303 Irminger Basins leads to the formation of regional mode waters: the Iceland Subpolar Mode Water (IcSPMW, S
304 $= 35.2$, $\theta^\circ = 8.0$ °C) and the Irminger Subpolar Mode Water (IrSPMW, $S = 35.01$, $\theta^\circ = 5.0$ °C), respectively.
305 IcSPMW was a relatively warm water mass with potential temperature up to 7 °C (García-Ibáñez et al., 2015).
306 Another branch of the NAC mixed with Labrador Current waters to form the relatively fresh SubArctic
307 Intermediate Water (SAIW, $S = 34.8$, 4.5 °C $< \theta^\circ < 6$ °C).

308 The Irminger Basin is a complex area with a multitude of water masses. In the middle of the basin, an old LSW,
309 formed one year before (Straneo et al., 2003), spread between 500 and 1200 m depth. Close to the bottom, the

310 Denmark Strait Overflow Water (DSOW, $S = 34.91$) flowed across the basin. Greenland coastal waters were
311 characterised by low salinity values, down to $S = 33$. The strong East Greenland Current (EGC) flowed southward
312 along the Greenland shelf in the Irminger Basin. At the southern tip of Greenland, this current enters the Labrador
313 Basin along the west coast of Greenland and followed the outline of the basin until the Newfoundland shelf. In
314 the Labrador Basin, the deep convection of SPMW at 2000 m was involved in the formation of the LSW ($S =$
315 34.9 , $\theta^{\circ} = 3.0^{\circ}\text{C}$) (García-Ibáñez et al., 2015; Yashayaev and Loder, 2009). Above the Newfoundland Shelf,
316 surface waters were affected by discharge from rivers and ice-melting and characterised by extremely low salinity
317 for open ocean waters, below 32 in the first 15 meters.

318 3.2. Section overview

319 Total particulate concentrations spanned a large range of concentrations from below detection (Table 1) to 304
320 nmol L^{-1} for PFe, 1544 nmol L^{-1} for PAI, 3.5 nmol L^{-1} for PMn and 402 nmol L^{-1} for PP. The ranges of
321 concentrations are comparable to other studies recently published (Table 2).

322 Along the section, PFe, PAI, and PMn were predominantly found ($> 90\%$) in particles larger than $5 \mu\text{m}$, except
323 in surface waters, reflecting a more heterogenous pattern, where $9 \pm 8.6\%$ of PFe, $10.9 \pm 15.4\%$ of PAI and 32.8
324 $\pm 16.6\%$ of PMn, $38.8 \pm 8.6\%$ of PP were hosted by smaller particles ($0.45\text{-}5 \mu\text{m}$). Data are shown in Figure 3.

325

326 3.3. Open Ocean stations: from the Iberian Abyssal Plain to the Labrador Basin

327 This concerns all stations from station 11 to 77, with the exception of stations 53, 56 and 61 which were sampled
328 close to the Greenland coast (Figure 1). Particulate iron concentration profiles showed identical patterns at all the
329 open ocean stations encountered along the section. Median PFe was low at 0.25 nmol L^{-1} within the first 100 m
330 and steadily increased with depth. However, at two stations, elevated concentrations were determined in the upper
331 100 m, up to 4.4 nmol L^{-1} at station 77 at 40 m depth and 7 nmol L^{-1} at station 63 between 70 and 100 m depth.
332 PFe concentrations gradually increased with depth, with a median PFe of 1.74 nmol L^{-1} below 1000m. Close to
333 the seafloor of some stations (26, 29, 32, 34, 49, 60, and 71), high concentrations of PFe were observed, up to 88
334 nmol L^{-1} (station 71 at 3736 m). These high PFe values were associated with low beam transmissometry values \leq
335 97% .

336 Particulate aluminium and manganese profiles were similar to PFe profiles, with low concentrations measured in
337 the first 100 m (1.88 nmol L^{-1} and 55 pmol L^{-1} , respectively) which increased towards the seafloor. Close to the
338 seafloor, high concentrations were determined at the same stations cited above for PFe, with a maximum of 264
339 nmol L^{-1} and 3.5 nmol L^{-1} for PAI and PMn respectively at station 71 (supplementary Table S1). Highest
340 particulate phosphorus concentrations were in the uppermost 50 m, with a median value of 66 nmol L^{-1} . Below
341 200 m depth PP concentrations decreased to values below 10 nmol L^{-1} . Inter-basins differences were observed
342 within surface samples, with median PP concentration being higher in the Irminger Basin (127 nmol L^{-1}) than in
343 the Iberian Abyssal Plain (28 nmol L^{-1}) (Figure 3).

344 Finally, above the Reykjanes Ridge, PP, PMn, PAI and PFe concentrations were in the same range as the
345 surrounding open ocean stations. However, close to the seafloor, high concentrations were measured, with PFe,

346 PAI, and PMn reaching 16.2 nmol L⁻¹, 28.8 nmol L⁻¹, and 0.51 nmol L⁻¹ at 1354 m depth, respectively (Figure 3
347 and Table S1).

348

349 *3.4. Margins and Shelves: Iberian Margin (stations 1 to 4), Greenland coast (stations 53, 56*
350 *and 61) and Newfoundland Shelf (station78)*

351

352 The Iberian margin was characterised by low beam transmissometry values at station 2 (88 % at 140 m depth,
353 Figure 4a) suggesting high particle concentrations. Particulate iron concentrations varied from 0.02 nmol L⁻¹ to
354 304 nmol L⁻¹. Within the first 50 m, PFe concentrations decreased towards the shelf break where PFe dropped
355 from 2.53 nmol L⁻¹ (station 2) to 0.8 nmol L⁻¹ (Station 1). At all three stations, PFe concentrations increased with
356 depth and reached a maximum close to the seafloor. For example, 300 nmol L⁻¹ of PFe was determined at 138.5
357 m depth at station 2. Lithogenic tracers, such as PAI or PMn, presented similar profiles to PFe with concentrations
358 ranging from 0.11 and 1544 nmol L⁻¹, and from below detection limit to 2.51 nmol L⁻¹, respectively (Figure 3,
359 Table S1). Total particulate phosphorus concentrations were relatively low in surface waters ranging from values
360 below detection to 38 nmol L⁻¹; concentrations decreased with depth and were less than 0.7 nmol L⁻¹ below 1000
361 m depth.

362 In the vicinity of the Greenland shelf, PFe concentrations had a high median value of 10.8 nmol L⁻¹ and were
363 associated with high median PAI and PMn concentrations of 32.3 nmol L⁻¹ and 0.44 nmol L⁻¹, respectively.
364 Concentrations of PP were high at the surface with a value of 197 nmol L⁻¹ at 25 m depth of station 61. Then, PP
365 concentrations decreased strongly, to less than 30 nmol L⁻¹ below 100 meters depth. Furthermore, beam
366 transmissometry values in surface waters at these three stations, were the lowest of the entire section, with values
367 below 85 % (Figure 4a).

368 Close to the Newfoundland margin, surface waters displayed a small load of particulate trace metals as PFe, PAI,
369 and PMn concentrations were below 0.8 nmol L⁻¹, 2 nmol L⁻¹, and 0.15 nmol L⁻¹, respectively. Then, close to the
370 bottom of station 78, at 371 m depth, beam transmissometry values dropped to 94 % (Figure 4a) and were
371 associated with extremely high concentrations of PFe = 168 nmol L⁻¹, PAI = 559 nmol L⁻¹, and PMn = 2 nmol L⁻¹.
372 Total PP concentrations in the first 50 m ranged from 35 to 97 nmol L⁻¹. Below 50 m, PP remained relatively
373 high with values up to 16 nmol L⁻¹ throughout the water column. (Figure 3 and Table S1).

374

375 **4. Discussion**

376 Our goal was to investigate mechanisms that drive the distribution of PFe in the North Atlantic, in particular the
377 different routes of supply and removal. Possible sources of PFe include lateral advection offshore from margins,
378 atmospheric inputs, continental run-off, melting glaciers and icebergs, resuspended sediments, hydrothermal
379 inputs and biological uptake. Removal processes include remineralization, dissolution processes and sediment
380 burial.

381 In the following sections, we examine each of these sources and processes, explore the evidence for their relative
382 importance, and use compositional data to estimate the particle types and host phases for iron and associated
383 elements.

384 *4.1. Analysis of the principal factors controlling variance: near-ubiquitous influence of crustal*
385 *particles in the water column*

386 Positive matrix factorisation analysis (Figure 5) was undertaken on the entire dataset, in consequence, the factors
387 described below are highly influenced by the major variations of particulate element concentrations (usually at
388 the interfaces, i.e. margin, seafloor, surface layer). The first factor is characterised by lithogenic elements,
389 representing 86.8 % of the variance of PFe, 75.8 % of PAI and 90.5 % of PTi. The second factor is correlated with
390 both Mn and Pb and explains no less than 76.5 % and 77.0 % of their respective variances. Ohnemus and Lam
391 (2015) observed this co-relation between manganese and lead particles and explained it by the co-transport on
392 Mn-oxides (Boyle et al., 2005). The formation of barite explains the third factor and constrained 87.7 % of the Ba
393 variance in the studied regions. Biogenic barite accumulation within the mesopelagic layer is related to bacterial
394 activity and remineralisation of biogenic material (Lemaitre et al., 2018a). A biogenic component is the fourth
395 factor and explained most of PP variance, 83.7 %. The micronutrient trace metals, copper, cobalt and zinc, had
396 more than a quarter of their variances influenced by this factor. Note that the biogenic contribution to PFe and
397 other trace elements will be discussed in another paper (Planquette et al., in prep).

398 These results indicate that along the GA01 section, PFe distributions were predominantly controlled by lithogenic
399 material and to a smaller extent by remineralisation processes (~~as seen by a factor 3 contribution of 4.1 % PMF,~~
400 ~~factor 3 = 4.1 %~~). This does not rule out some biogenic influences on PFe distribution, especially in the surface,
401 but ~~this-its~~ contribution is ~~most likely~~ obscured by the high lithogenic contribution.

402 To further investigate the influence of crustal material on the distribution of PFe, it is instructive to examine the
403 distribution of the PFe to PAI molar ratio, and the resulting %PFe_{litho} (see section 2.6 for definition of this
404 parameter) along the section (Figure 6). Overall, the estimated lithogenic contribution to PFe varies from 25 %
405 (west of the Irminger Basin, station 60, 950 m depth) to 100 % at stations located within the Western European
406 Basin. Note that 100% of estimated lithogenic PFe does not necessary mean that biogenic particles are absent;
407 they may just be masked by the dominance of lithogenic particles. Important inter-basin variations are observed
408 along the section (Figure 6). The IAP and WEB ~~are linked with displayed~~ high median values of the proxy
409 %PFe_{litho}, 90 % (Figure 6b); ~~which is also reflected in the MW and NEADW PFe/PAI ratio which displays a~~
410 ~~value close to the crustal one (Figure 7).~~ This could be linked to the lateral advection of iron rich lithogenic
411 particles sourced from the Iberian margin and to atmospheric inputs (Shelley et al., 2017). ~~The atmospheric~~
412 ~~external source is discussed in more detail in section 4.2.4.~~ Then, between stations 26 and 29, the %PFe_{litho} proxy
413 values dramatically decreased, and reached values less than 55 % in the Iceland, Irminger and the Labrador basins
414 (Figure 6b). This feature is likely associated with the presence of the Sub-Arctic Front, located between 49.5 and
415 51 °N latitude and 23.5 and 22 °W longitude (Zunino et al., 2017). Indeed, this front which separates cold and
416 fresh water of subpolar origin from warm and salty water of subtropical origin was clearly identifiable by the
417 steep gradient of the isohalines between station 26 and 29; salinity dropping from 35.34 to 35.01 (Figure 2). ~~North~~
418 ~~of the Sub-Arctic Front, LSW and ISOW display high PFe/PAI ratios, ranging from 0.36 to 0.44 mol mol⁻¹ (Figure~~
419 ~~6a). These high ratios, compared to the crustal one (i.e. 0.2) Lower %PFe_{litho} proxy values), could be associated~~
420 with higher proportions of PFe from biogenic origin, especially in the case of the LSW.

421
422 *4.2. Tracking the different inputs of particulate iron*

423

4.2.1. Inputs at margins: Iberian, Greenland and Newfoundland

424 Inputs of iron from continental margin sediments supporting the high productivity found in shallow coastal regions
425 have been demonstrated in the past (e.g. Cullen et al. 2009, Elrod et al. 2004, Jeandel et al. 2011, Ussher et al.
426 2007) and sometimes, were shown to be advected at great distances from the coast (e.g. Lam and Bishop, 2008).
427 In the following section, we will investigate these possible sources in proximity to the different margins
428 encountered.

429

430 *The Iberian margin*

431 The Iberian margin was an important source of lithogenic-derived iron-rich particles to the Atlantic Ocean during
432 GEOVIDE; shelf resuspension impacts were perceptible up to 280 km from the margin (Station 11) in the Iberian
433 Abyssal Plain (Figure 8).

434 On the shelf, at station 2, high sediment resuspension resulted in the low beam transmissometry value (87.6 %) at
435 the immediate vicinity of the seafloor (153 m depth). This sediment resuspension led to an extensive input of
436 lithogenic particles within the water column associated with high concentrations of PFe (304 nmol L⁻¹), PAI (1500
437 nmol L⁻¹), and PMn (2.5 nmol L⁻¹) (Figure 3, Table S1). Moreover, 100 % of PFe was estimated to have a
438 lithogenic origin (Figure 8b) while 100 % of the PMn was estimated to be the result of a recent sediment
439 resuspension according to the %PFe_{litho} and “%bulk sediment Mn” proxies (Figure 8b and c), confirming the
440 resuspended particle input. In addition, ADCP data acquired during GEOVIDE (Zunino et al., 2017) and several
441 other studies have reported an intense current spreading northward coming from the Straits of Gibraltar and
442 Mediterranean Sea, leading to the strong resuspension of benthic sediments above the Iberian Shelf (e.g. Biscaye
443 and Eittrheim, 1977, Eittrheim et al., 1976, McCave and Hall, 2002, Spinrad et al., 1983).

444 At distance from the shelf, within the Iberian Abyssal Plain, an important lateral advection of PFe from the margin
445 was observable (Figure 8a). These lateral inputs occurred at two depth ranges: between 400 and 1000 m as seen
446 at stations 4 and 1, with PFe concentrations reaching 4 nmol L⁻¹, and between 2500 m and the bottom (3575 m)
447 of station 1, with PFe concentrations reaching 3.5 nmol L⁻¹. While 100 % of PFe had a lithogenic signature, the
448 sedimentary source input estimation decreased, between 40 % and 90 % of the PMn (Figure 8b). Transport of
449 lithogenic particles was observable until station 11 (12.2°W) at 2500 m where PFe concentration was 7.74 nmol
450 L⁻¹ and 60 % of PMn had a sedimentary origin (Figure 4). It is noteworthy that no increase in PFe, PMn or PAI
451 was observed between 500 and 2000 m depth, where the MOW spreads (García-Ibáñez et al., 2015). This is
452 consistent with the observed dissolved iron (DFe) concentrations (Tonnard et al., 2018, this issue), yet in contrast
453 to dissolved aluminium (DAI) concentrations (Menzel-Barraqueta et al., 2018, this issue) which were high in the
454 MOW, and with the study of Ohnemus and Lam (2015) that reported a maximum PFe concentration at 695 m
455 depth associated with the particle-rich Mediterranean Overflow Water (Eittrheim et al., 1976) in the IAP. However,
456 their station was located further south of our station 1. The shallower inputs observed at stations 1 and 4 could
457 therefore be attributed to sediment resuspension from the Iberian margin and nepheloid layer at depth for station
458 1.

459 Surface coastal waters of the Iberian Shelf are impacted by the runoff for the Tagus River, which is characterised
460 by high suspended matter discharges, ranging between 0.4 to 1 × 10⁶ tons yr⁻¹, and with a high anthropogenic
461 trace element signature (Jouanneau et al., 1998). During the GEOVIDE section, the freshwater input was

462 observable at stations 1, 2 and 4 in the first 20 m; salinity was below 35.2 while surrounding water masses had
463 salinity up to 35.7. Within the freshwater plume, particulate concentrations were high at station 2 with PFe of 1.83
464 nmol L^{-1} . Further away from the coast, the particulate concentrations remained low at 20m depth, with PFe, PAI,
465 and PMn concentrations of 0.77 nmol L^{-1} , 3.5 nmol L^{-1} , and 0.04 nmol L^{-1} , respectively at station 1. The low
466 expansion of the Tagus plume is likely due to the rapid settling of suspended matter. Indeed, our coastal station 2
467 was located approximately 50 km from the Iberian coast, whereas the surface particle load can only be observed
468 at a maximum distance of 30 km from the Tagus estuary (Jouanneau et al., 1998). Overall, the Iberian margin
469 appears to be an important source of lithogenic-derived iron rich particles ~~to~~ the Atlantic Ocean.

471 *South Greenland*

472 During GEOVIDE, the Greenland shelves were a source of particulate-rich meteoric water leading to a transfer
473 of DFe to PFe by enhanced biological activity. Indeed, both East (station 53) and West (station 61) Greenland
474 shelves had high concentration of particles (beam transmissometry of 83 %, Figure 4a) and particulate trace
475 elements, reaching 22.1 nmol L^{-1} (at 100 m depth) and 18.7 nmol L^{-1} (at 136 m depth) of PFe, respectively. Several
476 studies have already demonstrated the importance of icebergs and sea ice melting as sources of dissolved and
477 particulate iron (e.g. van der Merwe et al., 2011a, 2011b; Planquette et al., 2011; Raiswell et al., 2008). The
478 Greenland shelf is highly influenced by external fresh water inputs such as sea-ice-melting or riverine runoff
479 (Fragoso et al., 2016), which are important sources of iron to the Greenland Shelf (Bhatia et al., 2013; Hawkings
480 et al., 2014; Statham et al., 2008). During the cruise, the relative freshwater observed ($S < 33$ psu) within the first
481 25 m of stations 53 and 61 was associated with high PFe (19 nmol L^{-1}), PAI (61 nmol L^{-1}), PMn (0.6 nmol L^{-1})
482 and low beam transmissometry ($\leq 85\%$) (Figure 4a and Table S1). The associated particles were enriched in iron
483 compared to aluminium, as PFe/PAI ratio was 0.3 within the meteoric water plume. The high PP concentrations
484 (reaching 197 nmol L^{-1}) resulting from high biological production (Chl-a = 6.21 mg m^{-3} at 24 m at station 61),
485 induced by the supply of bioavailable dissolved iron (surface DFe of 0.79 nM at station 61) from meteoric water
486 (Raiswell et al., 2008; Statham et al., 2008; Tonnard et al. 2018), led to a transfer of DFe to the particulate phase.
487 This is in line with the finding that around 30 % PFe had a non-lithogenic origin. In addition, only 40% PMn
488 originated from resuspended sediments. Interestingly, these two proxies remained constant from the seafloor to
489 the surface (Station 49, Figure 8), with around 25 % of the PMn of sedimentary origin, which could be due to
490 important mixing occurring on the shelf. The lithogenic PFe could result from the release of PFe from Greenland
491 bedrock captured during the ice sheet formation on land.

492 The spatial extent of the off-shelf lateral transport of particles was not important on the east Greenland coast.
493 Indeed, no visible increase of particulate trace metal concentrations was visible at the first station off-shelf, station
494 60 (Figure 8), except at 1000 m depth, where a strong increase (up to 90 %) of sedimentary PMn was seen. This
495 is probably due to the East Greenland Coastal Current (EGCC) that was located at station 53 which constrained
496 these inputs while stations 56 and 60 were under the influence of another strong current, the East Greenland-
497 Irminger current (EGIC) (Zunino et al., 2017). To the west of the Greenland margin, lateral transport of particles
498 was slightly more important. Noticeable concentrations of particulate lithogenic elements were observable until
499 station 64 located 125 km away from shoreline. These particles had a decreased PFe lithogenic contribution (50
500 %) with a similar (25 %) sedimentary PMn content than closer to the margin (Figure 8b and c). The increasing

501 nature of non-lithogenic PFe is linked to the bloom in surface waters (PFe/PAI ratio of 0.30 mol mol⁻¹, PP of 197
502 nmol L⁻¹ and Chl-a concentration of 6.21 mg m⁻³ at station 61), with the gravitational settling of biogenic PFe.
503 Therefore, particles newly resuspended from Greenland sediments are an important source, representing around
504 one third of the pMn pool, combined with surface inputs such as riverine runoff and/or ice-melting that are
505 delivering particles on the shelf, and also biological production. Unlike the Iberian shelf, the Greenland margin
506 was not an important provider of particulate metals inside the Irminger and Labrador Basins, due to the circulation
507 that constrained the extent of the margin plume.

508
509

510 *The Newfoundland Shelf*

511 Previous studies have already described the influence of fresh water on the Newfoundland shelf from the Hudson
512 Strait and/or Canadian Arctic Archipelago (Fragoso et al., 2016; Yashayaev, 2007). Yashayaev (2007) also
513 monitored strong resuspension of sediments associated with the spreading of the Labrador Current along the West
514 Labrador margin.

515 Close to the Newfoundland coastline, at station 78, high fresh water discharge (≤ 32 psu) was observed in surface
516 waters (Benetti et al., 2017). Interestingly, these freshwater signatures were not associated with elevated
517 particulate trace metal concentrations. Distance of meteoric water sources implied a long travel time for the water
518 to spread through the Labrador Basin to our sampling stations. Along the journey, particles present originally may
519 have been removed from the water column by gravitational settling.

520 The proportion of lithogenic PFe was relatively high and constant throughout the water column, with a median
521 value of 70 %. At station 78, 95 % of the PMn had a sedimentary origin close to the seafloor (371 m). The
522 spreading of the recent sediment resuspension was observable until 140 m depth where the contribution of
523 sedimentary Mn was still 51% (Figure 8c, Table S2). This could correspond to an intense nepheloid layer as
524 previously reported by Biscaye and Eittrheim (1977) (see also section 3.3.2). The high PFe concentration (184
525 nmol L⁻¹, station 78, 371 m depth, Figure 8b) associated with a high percentage of sedimentary PMn (95%)
526 observed at the bottom of this station, was therefore the result of an important resuspension of shelf sediments.
527 This was confirmed with low transmissometry values of 95 % (Figure 4a).

528

529 ~~The important phytoplanktonic community present (maximum Chl a= 4.91 mg m⁻³, Tonnard et al., in prep), is
530 linked to a low PFe concentration of 0.79 nmol L⁻¹ at 10 m depth, but, with a high PFe/PAI ratio, up to 0.4, and
531 PP concentration of 97 nmol L⁻¹, confirming the biological influence. Either the biogenic particles settled quickly,
532 and/or they were quickly remineralized. Concerning this latter process, intense remineralization at station 77 (7
533 mmol C m⁻² d⁻¹ compared to 4 mmol C m⁻² d⁻¹ in the Western European Basin) has been reported by Lemaitre et
534 al. (2018a and 2018b), which could explain the low PFe values throughout the water column.~~

535 Along the GEOVIDE section, continental shelves provided an important load of particles to the surrounding water
536 column. The three margins sampled during GEOVIDE behaved very differently; the Iberian margin discharged
537 high quantities of lithogenic particles far from the coast while the Greenland and Newfoundland margins did not
538 reveal important PFe concentrations. Spreading of particles is tightly linked to hydrodynamic conditions, which
539 in the case of the Greenland margin, prevented long distance seeding of PFe. Moreover, each margin showed a
540 specific PFe/PAI ratio (Figure 9) indicating different composition of the resuspended particles. Resuspended

541 particles represent the composition of sediment at the margin if redox transformation of iron and aluminium are
542 considered negligible under these circumstances. Differences between margins were due to the presence of non-
543 crustal particles, either biogenic or authigenic. Biological production in surface waters and authigenic formation
544 of iron hydroxide produced particles with a higher PFe/PAI content and their export through the water column to
545 the sediment increased the PFe/PAI ratio at depth. Regions where biological production is intense such as in the
546 vicinity of Newfoundland presented higher PFe/PAI ratios of resuspended benthic particles.

547

548

4.2.2 Benthic resuspended sediments

549 Along the GEOVIDE section, Benthic nepheloid layers (BNLs) provided high concentrations of particulate trace
550 elements to the deep open ocean, contributing significantly to the total budget of iron. BNLs were observable in
551 each province, although intensities varied (Figures 3 and 10).

552 In BNLs located within the WEB, PFe concentrations reached up to 10 nmol L^{-1} (stations 26 and 29, Figure 10a;
553 Table S1). These concentrations were lower than PFe concentrations in BNLs from the Icelandic (stations 32 and
554 34), Irminger (stations 42 and 44) and Labrador Basins (stations 68, 69 and 71), where benthic resuspension led
555 to PFe concentrations higher than 40 nmol L^{-1} , even reaching 89 nmol L^{-1} at the bottom of station 71 (3736 m
556 depth). Moreover, in the Irminger and Labrador Basins, PFe/PAI molar ratios within BNLs were higher than the
557 ones measured within the WEB at station 26 and 29. In the Irminger Basin, PFe/PAI reached 0.4 mol mol^{-1} (Figure
558 10b), which could reveal a mixture of lithogenic and biogenic matter that had been previously exported. This
559 feature was also observed in the Labrador Basin, with PFe/PAI ratio ranging between 0.34 and $0.44 \text{ mol mol}^{-1}$. In
560 contrast, BNLs sampled in the WEB clearly have a lithogenic imprint, with PFe/PAI molar ratios close to the
561 crustal one. Resuspended sediments with a non-crustal contribution seem to have higher PFe contents than
562 sediments with lithogenic characteristics. Nevertheless, interestingly all BNLs present during GEOVIDE were
563 spreading identically, with impacts observable up to 200 m above the oceanic seafloor (Figure 10), as reflected in
564 beam transmissometry values, and PFe concentrations, which returned to background levels at 200 m above the
565 seafloor. The presence of these BNLs has also been reported by Le Roy et al. (2018) using radium-226 activity.
566 Important differences of PFe intensities could also be due to different hydrographic components and topographic
567 characteristics. BNLs occur due to strong hydrographic stresses (i.e. boundary currents, benthic storms and deep
568 eddies) interacting with the ocean floor (Biscaye and Eittrheim, 1977; Eittrheim et al., 1976; Gardner et al., 2017,
569 2018). They are, by definition, highly variable geographically and temporally, but we have no physical data which
570 would allow us to investigate this hypothesis further.

571

572

4.2.3. Reykjanes Ridge inputs

573 Above the Reykjanes Ridge (Station 38), high PFe concentrations were determined, reaching 16 nmol L^{-1} just
574 above the seafloor, while increased DFe concentrations were reported to the east of the ridge (Tonnard et al.,
575 2018, this issue). The exact sources of iron-rich particles cannot be well constrained, as they could come from
576 active hydrothermal vents or resuspension of particulate matter from new crustal matter produced at the ridge.
577 According to the oceanic circulation (Zunino et al., 2017; Garcia-Ibanez et al., 2017), hydrothermal particles could
578 have been seen in the ISOW within the Icelandic Basin. Nevertheless, at the vicinity of the ridge, scanning electron
579 microscope (SEM) analyses of our samples did reveal several biological debris and clays but not the presence of

580 iron (oxy-)hydroxide particles (supplementary figure S1), which are known to be produced close to hydrothermal
581 vents (Elderfield and Schultz, 1996). Their absence could thus indicate an absence of vents. However, data from
582 other proxies, such as helium-3, would be necessary to confirm the presence or absence of an hydrothermal source
583 close to station 38.

584

585

4.2.4. Atmospheric inputs

586 Atmospheric deposition is an important source of trace elements in surface of the open ocean (e.g. Jickells et al.,
587 2005). Atmospheric inputs, both wet and dry, were reported to be low during the GEOVIDE cruise (Menzel
588 Barraqueta et al., 2018b, this issue; Shelley et al., 2017; 2018). In fact, oceanic particle measurements in surface
589 waters along the section did not reveal high PFe or PAI concentrations. One pattern is interesting to note: the
590 surface waters of the Iberian Abyssal Plain and Western European Basin, between stations 11 and 23 presented a
591 characteristic feature with really low PFe/PAI elemental ratios, of 0.11, smaller than the UCC ratio of 0.21 (Figure
592 6a). Such low ratios have been reported in the same region by Barrett et al. (2012). One possible explanation is
593 given by Buck et al. (2010) who described Fe-depleted aerosols in this area of the North Atlantic with PFe/PAI
594 ratio below UCC ratio. However, Shelley et al. (2017) found a higher PFe/PAI ratio around 0.25 in this area (their
595 samples geo5-6). This result, highlights some of the difficulties in linking atmospheric inputs to water column
596 data (Baker et al., 2016), and implies a probable fractionation after aerosol deposition. In addition, there is high
597 spatial and temporal variability of atmospheric deposition (Mahowald et al., 2005) and a certain degree of
598 uncertainty about the dissolution processes of atmospherically-transported particles (Bonnet and Guieu, 2004).

599

600

601

5. Conclusions

602

603 The investigation of the PFe composition of suspended particulate matter along the GEOVIDE section in the
604 North Atlantic reflects the pervasive influence of crustal particles, augmented by sedimentary inputs at margins,
605 and within benthic nepheloid layers at depths. In consequence, variance of particulate iron along the section is
606 mainly explained by lithogenic factors.

607 Resuspension of sedimentary particles from continental shelves are responsible of high particulate iron
608 concentrations within the surrounding water column and could be observed at long distances from the shelf, in
609 the case of the Iberian margin. Our results also demonstrate the impact of Arctic meteoric water on the Greenland
610 shelf, while in surface waters, the enhancement of productivity by new bioavailable iron is leading to a transfer
611 of dissolved iron to the particulate phase. Benthic nepheloid layer are providing important concentration of
612 particles to the water column; they were observed in most of the oceanic basin encountered along the GEOVIDE
613 section.

614 Overall, PFe distributions in the North Atlantic are strongly influenced by sources at its boundaries (i.e.
615 continental margins and seafloor). When combined with other datasets from the GEOTRACES program in a
616 modelling study, for example, use of this data will facilitate a greater understanding of particulate iron cycling in
617 the North Atlantic.

618

619

620

621 **Acknowledgments**

622 We are greatly indebted to the captain and crew of the N/O Pourquoi Pas? for their help during the GEOVIDE
623 mission and clean rosette deployment. We would like to give special thanks to Fabien Pérault and Emmanuel de
624 Saint Léger for their technical expertise, to Catherine Schmechtig for the GEOVIDE database management and
625 Greg Cutter for his guidance in setting up the new French clean sampling system. We would like to thank both
626 reviewers for constructive comments that greatly improved this manuscript.

627 We also would like to thank Reiner Schlitzer for the Ocean Data View software (ODV).

628 This work was supported by the French National Research Agency (ANR-13-BS06-0014, ANR-12-PDOC-0025-
629 01), the French National Centre for Scientific Research (CNRS-LEFE-CYBER), the LabexMER (ANR-10-
630 LABX-19), and Ifremer. It was supported for the logistic by DT-INSU and GENAVIR.

631

632 **References**

633 Aguilar-Islas, A. M., Rember, R., Nishino, S., Kikuchi, T. and Itoh, M.: Partitioning and lateral transport of iron
634 to the Canada Basin, *Polar Sci.*, 7(2), 82–99, doi:10.1016/j.polar.2012.11.001, 2013.

635 Baker, A. R., Adams, C., Bell, T. G., Jickells, T. D. and Ganzeveld, L.: Estimation of atmospheric nutrient inputs
636 to the Atlantic Ocean from 50°N to 50°S based on large-scale field sampling: Iron and other dust-associated
637 elements, *Global Biogeochem. Cycles*, 27(3), 755–767, doi:10.1002/gbc.20062, 2013.

638 Baker, A. R., Landing, W. M., Bucciarelli, E., Cheize, M., Fietz, S., Hayes, C. T., Kadko, D., Morton, P. L.,
639 Rogan, N., Sarthou, G., Shelley, R. U., Shi, Z., Shiller, A. and van Hulst, M. M. P.: Trace element and isotope
640 deposition across the air–sea interface: progress and research needs, *Philos. Trans. R. Soc. A Math. Phys. Eng.
641 Sci.*, 374(2081), 20160190, doi:10.1098/rsta.2016.0190, 2016.

642 Barrett, P. M., Resing, J. A., Buck, N. J., Buck, C. S., Landing, W. M. and Measures, C. I.: The trace element
643 composition of suspended particulate matter in the upper 1000m of the eastern North Atlantic Ocean: A16N, *Mar.
644 Chem.*, 142–144, 41–53, doi:10.1016/j.marchem.2012.07.006, 2012.

645 Benetti, M., Reverdin, G., Lique, C., Yashayaev, I., Holliday, N. P., Tynan, E., Torres-Valdes, S., Lherminier, P.,
646 Tréguer, P., and Sarthou, G.: Composition of freshwater in the spring of 2014 on the southern Labrador shelf and
647 slope, *Journal of Geophysical Research: Oceans*, 122, 1102–1121, 10.1002/2016jc012244, 2017.

648 Berger, C. J. M., Lippiatt, S. M., Lawrence, M. G. and Bruland, K. W.: Application of a chemical leach technique
649 for estimating labile particulate aluminum, iron, and manganese in the Columbia River plume and coastal waters
650 off Oregon and Washington, *J. Geophys. Res.*, 113, C00B01, doi:10.1029/2007JC004703, 2008.

651 Bergquist, B. A., Wu, J. and Boyle, E. A.: Variability in oceanic dissolved iron is dominated by the colloidal
652 fraction, *Geochim. Cosmochim. Acta*, 71(12), 2960–2974, doi:10.1016/j.gca.2007.03.013, 2007.

653 Bhatia, M. P., Kujawinski, E. B., Das, S. B., Breier, C. F., Henderson, P. B. and Charette, M. A.: Greenland
654 meltwater as a significant and potentially bioavailable source of iron to the ocean, *Nat. Geosci.*, 6(4), 274–278,
655 doi:10.1038/ngeo1746, 2013.

656 Biscaye, P. E. and Eitrem, S. L.: Suspended Particulate Loads and Transports in the Nepheloid Layer of the
657 Abyssal Atlantic Ocean, *Dev. Sedimentol.*, 23(C), 155–172, doi:10.1016/S0070-4571(08)70556-9, 1977.

658 Bishop, J. K. B. and Biscaye, P. E.: Chemical characterization of individual particles from the nepheloid layer in
659 the Atlantic Ocean, *Earth Planet. Sci. Lett.*, 58(2), 265–275, doi:10.1016/0012-821X(82)90199-6, 1982.

660 Bishop, J. K. B. and Fleisher, M. Q.: Particulate manganese dynamics in Gulf Stream warm-core rings and
661 surrounding waters of the N.W. Atlantic, *Geochim. Cosmochim. Acta*, 51(10), 2807–2825, doi:10.1016/0016-
662 7037(87)90160-8, 1987.

663 Bonnet, S. and Guieu C.: Dissolution of atmospheric iron in seawater, *Geophys. Res. Lett.*, 31(3), L03303,
664 doi:10.1029/2003GL018423, 2004.

665 Boyle, E. A., Bergquist, B. A., Kayser, R. A. and Mahowald, N.: Iron, manganese, and lead at Hawaii Ocean
666 Time-series station ALOHA: Temporal variability and an intermediate water hydrothermal plume, *Geochim.*
667 *Cosmochim. Acta*, 69(4), 933–952, doi:10.1016/j.gca.2004.07.034, 2005.

668 Buck, C. S., Landing, W. M., Resing, J. A. and Measures, C. I.: The solubility and deposition of aerosol Fe and
669 other trace elements in the North Atlantic Ocean: Observations from the A16N CLIVAR/CO2repeat hydrography
670 section, *Mar. Chem.*, 120(1–4), 57–70, doi:10.1016/j.marchem.2008.08.003, 2010.

671 Cheize, M., Planquette, H. F., Fitzsimmons, J. N., Pelleter, E., Sherrell, R. M., Lambert, C., Bucciarelli, E.,
672 Sarthou, G., Le Goff, M., Liorzou, C., Chéron, S., Viollier, E., and Gayet, N.: Contribution of resuspended
673 sedimentary particles to dissolved iron and manganese in the ocean: An experimental study, *Chemical Geology*.
674 doi: 10.1016/j.chemgeo.2018.10.003, 2018.

675 Collier, R. and Edmond, J.: The trace element geochemistry of marine biogenic particulate matter, *Prog.*
676 *Oceanogr.*, 13(2), 113–199, doi:10.1016/0079-6611(84)90008-9, 1984.

677 Cullen, J. T., Chong, M. and Ianson, D.: British columbia continental shelf as a source of dissolved iron to the
678 subarctic northeast Pacific Ocean, *Global Biogeochem. Cycles*, 23(4), 1–12, doi:10.1029/2008GB003326, 2009.

679 Cutter, G. A. and Bruland, K. W.: Rapid and noncontaminating sampling system for trace elements in global
680 ocean surveys, *Limnol. Oceanogr. Methods*, 10(JUNE), 425–436, doi:10.4319/lom.2012.10.425, 2012.

681 Dammshäuser, A., Wagener, T., Garbe-Schönberg, D. and Croot, P.: Particulate and dissolved aluminum and
682 titanium in the upper water column of the Atlantic Ocean, *Deep. Res. Part I Oceanogr. Res. Pap.*, 73, 127–139,
683 doi:10.1016/j.dsr.2012.12.002, 2013.

684 Dehairs, F., Jacquet, S., Savoye, N., Van Mooy, B. A. S., Buesseler, K. O., Bishop, J. K. B., Lamborg, C. H.,
685 Elskens, M., Baeyens, W., Boyd, P. W., Casciotti, K. L. and Monnin, C.: Barium in twilight zone suspended
686 matter as a potential proxy for particulate organic carbon remineralization: Results for the North Pacific, *Deep.*
687 *Res. Part II Top. Stud. Oceanogr.*, 55(14–15), 1673–1683, doi:10.1016/j.dsr2.2008.04.020, 2008.

688 Dutay, J. C., Tagliabue, A., Kriest, I. and van Hulst, M. M. P.: Modelling the role of marine particle on large
689 scale ^{231}Pa , ^{230}Th , Iron and Aluminium distributions, *Prog. Oceanogr.*, 133, 66–72,
690 doi:10.1016/j.pocean.2015.01.010, 2015.

691 Eitrem, S., Thorndike, E. M. and Sullivan, L.: Turbidity distribution in the Atlantic Ocean, *Deep. Res. Oceanogr.*
692 *Abstr.*, 23(12), 1115–1127, doi:10.1016/0011-7471(76)90888-3, 1976.

693 Elderfield, H. and Schultz, A.: Mid-Ocean Ridge Hydrothermal Fluxes and the Chemical Composition of the
694 Ocean, *Annu. Rev. Earth Planet. Sci.*, 24(1), 191–224, doi:10.1146/annurev.earth.24.1.191, 1996.

695 Ellwood, M. J., Nodder, S. D., King, A. L., Hutchins, D. A., Wilhelm, S. W. and Boyd, P. W.: Pelagic iron cycling
696 during the subtropical spring bloom, east of New Zealand, *Mar. Chem.*, 160, 18–33,
697 doi:10.1016/j.marchem.2014.01.004, 2014.

698 Elrod, V. A., Berelson, W. M., Coale, K. H. and Johnson, K. S.: The flux of iron from continental shelf sediments:
699 A missing source for global budgets, *Geophys. Res. Lett.*, 31(12), 2–5, doi:10.1029/2004GL020216, 2004.

700 Fitzwater, S. E., Johnson, K. S., Gordon, R. M., Coale, K. H. and Smith, W. O.: Trace metal concentrations in
701 the Ross Sea and their relationship with nutrients and phytoplankton growth, *Deep. Res. Part II Top. Stud.*
702 *Oceanogr.*, 47(15–16), 3159–3179, doi:10.1016/S0967-0645(00)00063-1, 2000.

703 Fragoso, G. M., Poulton, A. J., Yashayaev, I. M., Head, E. J. H., Stinchcombe, M. C. and Purdie, D. A.:
704 Biogeographical patterns and environmental controls of phytoplankton communities from contrasting
705 hydrographical zones of the Labrador Sea, *Prog. Oceanogr.*, 141, 212–226, doi:10.1016/j.pocean.2015.12.007,
706 2016.

707 Frew, R. D., Hutchins, D. A., Nodder, S., Sanudo-Wilhelmy, S., Tovar-Sanchez, A., Leblanc, K., Hare, C. E. and
708 Boyd, P. W.: Particulate iron dynamics during FeCycle in subantarctic waters southeast of New Zealand, *Global*
709 *Biogeochem. Cycles*, 20(1), 1–15, doi:10.1029/2005GB002558, 2006.

710 García-Ibáñez, M. I., Pardo, P. C., Carracedo, L. I., Mercier, H., Lherminier, P., Ríos, A. F. and Pérez, F. F.:
711 Structure, transports and transformations of the water masses in the Atlantic Subpolar Gyre, *Prog. Oceanogr.*, 135,
712 18–36, doi:10.1016/j.pocean.2015.03.009, 2015.

713 Gardner, W. D., Tucholke, B. E., Richardson, M. J. and Biscaye, P. E.: Benthic storms, nepheloid layers, and
714 linkage with upper ocean dynamics in the western North Atlantic, *Mar. Geol.*, 385, 304–327,
715 doi:10.1016/j.margeo.2016.12.012, 2017.

716 Gardner, W. D., Richardson, M. J. and Mishonov, A. V.: Global assessment of benthic nepheloid layers and
717 linkage with upper ocean dynamics, *Earth Planet. Sci. Lett.*, 482, 126–134, doi:10.1016/j.epsl.2017.11.008, 2018.

718 Gerringa, L. J. A., Rijkenberg, M. J. A., Schoemann, V., Laan, P. and de Baar, H. J. W.: Organic complexation
719 of iron in the West Atlantic Ocean, *Mar. Chem.*, 177, 434–446, doi:10.1016/j.marchem.2015.04.007, 2015.

720 Hawkings, J. R., Wadham, J. L., Tranter, M., Raiswell, R., Benning, L. G., Statham, P. J., Tedstone, A., Nienow,
721 P., Lee, K. and Telling, J.: Ice sheets as a significant source of highly reactive nanoparticulate iron to the oceans,
722 *Nat. Commun.*, 5(May), 1–8, doi:10.1038/ncomms4929, 2014.

723 Hwang, J., Druffel, E. R. M. and Eglinton, T. I.: Widespread influence of resuspended sediments on oceanic
724 particulate organic carbon: Insights from radiocarbon and aluminum contents in sinking particles, *Global
725 Biogeochem. Cycles*, 24(4), 1–10, doi:10.1029/2010GB003802, 2010.

726 Jeandel, C. and Oelkers, E. H.: The influence of terrigenous particulate material dissolution on ocean chemistry
727 and global element cycles, *Chem. Geol.*, 395, 50–66, doi:10.1016/j.chemgeo.2014.12.001, 2015.

728 Jeandel, C., Peucker-Ehrenbrink, B., Jones, M. T., Pearce, C. R., Oelkers, E. H., Godderis, Y., Lacan, F., Aumont,
729 O. and Arsouze, T.: Ocean margins: The missing term in oceanic element budgets?, *Eos, Transactions American
730 Geophysical Union*, 92(26), 217–224, doi: 10.1029/2011EO260001, 2011.

731 Jickells, T. D., An, Z. S., Andersen, K. K., Baker, A. R., Bergametti, C., Brooks, N., Cao, J. J., Boyd, P. W., Duce,
732 R. A., Hunter, K. A., Kawahata, H., Kubilay, N., LaRoche, J., Liss, P. S., Mahowald, N., Prospero, J. M.,
733 Ridgwell, A. J., Tegen, I. and Torres, R.: Global iron connections between desert dust, ocean biogeochemistry,
734 and climate, *Science* (80-.), 308(5718), 67–71, doi:10.1126/science.1105959, 2005.

735 Jouanneau, J. M., Garcia, C., Oliveira, A., Rodrigues, A., Dias, J. A. and Weber, O.: Dispersal and deposition of
736 suspended sediment on the shelf off the Tagus and Sado estuaries, S.W. Portugal, *Prog. Oceanogr.*, 42(1–4), 233–
737 257, doi:10.1016/S0079-6611(98)00036-6, 1998.

738 Labatut, M., Lacan, F., Pradoux, C., Chmeleff, J., Radic, A., Murray, J. W., Poitrasson, F., Johansen, A. M., Thil,
739 F., Lacan, F., Pradoux, C., Chmeleff, J., Radic, A., Murray, J. W., Poitrasson, F., Johansen, A. M. and Thil, F.:
740 Iron sources and dissolved-particulate interactions in the seawater of the Western Equatorial Pacific, iron isotope
741 perspectives., *Global Biogeochem Cycles*, 1044–1065, doi:10.1002/2014GB004928, 2014.

742 Lam, P. J. and Bishop, J. K. B.: The continental margin is a key source of iron to the HNLC North Pacific Ocean,
743 *Geophys. Res. Lett.*, 35(7), 1–5, doi:10.1029/2008GL033294, 2008.

744 Lam, P. J., Ohnemus, D. C. and Marcus, M. A.: The speciation of marine particulate iron adjacent to active and
745 passive continental margins, *Geochim. Cosmochim. Acta*, 80, 108–124, doi:10.1016/j.gca.2011.11.044, 2012.

746 Lam, P. J., Ohnemus, D. C. and Auro, M. E.: Size-fractionated major particle composition and concentrations
747 from the US GEOTRACES North Atlantic Zonal Transect, *Deep. Res. Part II Top. Stud. Oceanogr.*, 116, 303–
748 320, doi:10.1016/j.dsr2.2014.11.020, 2015.

749 Lam, P. J., Lee, J. M., Heller, M. I., Mehic, S., Xiang, Y. and Bates, N. R.: Size-fractionated distributions of
750 suspended particle concentration and major phase composition from the U.S. GEOTRACES Eastern Pacific Zonal
751 Transect (GP16), *Mar. Chem.*, (April), 0–1, doi:10.1016/j.marchem.2017.08.013, 2017.

752 Lannuzel, D., Bowie, A. R., van der Merwe, P. C., Townsend, A. T. and Schoemann, V.: Distribution of dissolved
753 and particulate metals in Antarctic sea ice, *Mar. Chem.*, 124(1–4), 134–146, doi:10.1016/j.marchem.2011.01.004,
754 2011.

755 Lannuzel, D., Van der Merwe, P. C., Townsend, A. T. and Bowie, A. R.: Size fractionation of iron, manganese
756 and aluminium in Antarctic fast ice reveals a lithogenic origin and low iron solubility, *Mar. Chem.*, 161, 47–56,
757 doi:10.1016/j.marchem.2014.02.006, 2014.

758 Lee, J. M., Heller, M. I. and Lam, P. J.: Size distribution of particulate trace elements in the U.S. GEOTRACES
759 Eastern Pacific Zonal Transect (GP16), *Mar. Chem.*, 201(September 2017), 108–123,
760 doi:10.1016/j.marchem.2017.09.006, 2017.

761 Lemaître, N., planquette, H., Planchon, F., Sarthou, G., Jacquet, S., Garcia-Ibanez, M. I., Gourain, A., Cheize,
762 M., Monin, L., Andre, L., Laha, P., Terryn, H., and Dehairs, F.: Particulate barium tracing significant mesopelagic
763 carbon remineralisation in the North Atlantic, *Biogeosciences*, doi:10.5194/bg-15-2289-2018, 2018a.

764 Lemaître, N., Planchon, F., Planquette, H., Dehairs, F., Fonseca-Batista, D., Roukaerts, A., Deman, F., Tang, Y.,
765 Mariez, C., and Sarthou G.: High variability of export fluxes along the North Atlantic GEOTRACES section
766 GA01: Particulate organic carbon export deduced from the 234Th method, *Biogeosciences*, doi:10.5194/bg-2018-
767 190, 2018b.

768 Le Roy, E., Sanial, V., Charette, M.A., Van Beek, P., Lacan, F., Jacquet, S.H., Henderson, P.B., Souhaut, M.,
769 García-Ibáñez, M.I., Jeandel, C. and Pérez, F.: The 226Ra-Ba relationship in the North Atlantic during
770 GEOTRACES-GA01, *Biogeosciences*, doi:10.5194/bg-2017-478, 2018.

771 Marsay, C. M., Lam, P. J., Heller, M. I., Lee, J. M. and John, S. G.: Distribution and isotopic signature of ligand-
772 leachable particulate iron along the GEOTRACES GP16 East Pacific Zonal Transect, *Mar. Chem.*, (November
773 2016), 1–14, doi:10.1016/j.marchem.2017.07.003, 2017.

774 Martin, J. H., Fitzwater, S. E., Michael Gordon, R., Hunter, C. N. and Tanner, S. J.: Iron, primary production and
775 carbon-nitrogen flux studies during the JGOFS North Atlantic bloom experiment, *Deep. Res. Part II*, 40(1–2),
776 115–134, doi:10.1016/0967-0645(93)90009-C, 1993.

777 McCave, I. N. and Hall, I. R.: Turbidity of waters over the Northwest Iberian continental margin, *Prog. Oceanogr.*,
778 52(2–4), 299–313, doi:10.1016/S0079-6611(02)00012-5, 2002.

779 Menzel Barraqueta, J.L., Schlosser, C., Planquette, H., Gourain, A., Cheize, M., Boutorh, J., Shelley, R., Pereira
780 Contreira, L., Gledhill, M., Hopwood, M.J. and Lherminier, P.: Aluminium in the North Atlantic Ocean and the

781 Labrador Sea (GEOTRACES GA01 section): roles of continental inputs and biogenic particle removal.
782 Biogeosciences, 1-28, doi: 10.5194/bg-2018-39, 2018.

783
784 Menzel Barraqueta, J.-L., Klar, J. K., Gledhill, M., Schlosser, C., Shelley, R., Planquette, H., Wenzel, B.,
785 Sarthou, G., and Achterberg, E. P.: Atmospheric aerosol deposition fluxes over the Atlantic Ocean: A
786 GEOTRACES case study, Biogeosciences Discuss., <https://doi.org/10.5194/bg-2018-209>, in review, 2018b.

787 Milne, A., Schlosser, C., Wake, B. D., Achterberg, E. P., Chance, R., Baker, A. R., Forryan, A. and Lohan, M.
788 C.: Particulate phases are key in controlling dissolved iron concentrations in the (sub)tropical North Atlantic,
789 Geophys. Res. Lett., 44(5), 2377–2387, doi:10.1002/2016GL072314, 2017.

790 Nuester, J., Shema, S., Vermont, A., Fields, D. M. and Twining, B. S.: The regeneration of highly bioavailable
791 iron by meso- and microzooplankton, Limnol Oceanogr, 59(4), 1399–1409, doi:10.4319/lo.2014.59.4.1399, 2014.

792 Oelkers, E. H., Jones, M. T., Pearce, C. R., Jeandel, C., Eiriksdottir, E. S. and Gislason, S. R.: Riverine particulate
793 material dissolution in seawater and its implications for the global cycles of the elements, Geosci., 344(11–12),
794 646–651, doi:10.1016/j.crte.2012.08.005, 2012.

795 Ohnemus, D. C. and Lam, P. J.: Cycling of lithogenic marine particles in the US GEOTRACES North Atlantic
796 transect, Deep. Res. Part II Top. Stud. Oceanogr., 116, 283–302, doi:10.1016/j.dsr2.2014.11.019, 2015.

797 Peers, G. and Price, N. M.: A role for manganese in superoxide dismutases and growth of iron-deficient diatoms,
798 Limnol. Oceanogr., 49(5), 1774–1783, doi:10.4319/lo.2004.49.5.1774, 2004.

799 Planquette, H. and Sherrell, R. M.: Sampling for particulate trace element determination using water sampling
800 bottles: Methodology and comparison to in situ pumps, Limnol. Oceanogr. Methods, 10(5), 367–388,
801 doi:10.4319/lom.2012.10.367, 2012.

802 Planquette, H., Fones, G. R., Statham, P. J. and Morris, P. J.: Origin of iron and aluminium in large particles (>
803 53 µm) in the Crozet region, Southern Ocean, Mar. Chem., 115(1–2), 31–42, doi:10.1016/j.marchem.2009.06.002,
804 2009.

805 Planquette, H., Sanders, R. R., Statham, P. J., Morris, P. J. and Fones, G. R.: Fluxes of particulate iron from the
806 upper ocean around the Crozet Islands: A naturally iron-fertilized environment in the Southern Ocean, Global
807 Biogeochem. Cycles, 25(2), doi:10.1029/2010GB003789, 2011.

808 Planquette, H., Sherrell, R. M., Stammerjohn, S. and Field, M. P.: Particulate iron delivery to the water column
809 of the Amundsen Sea, Antarctica, Mar. Chem., 153, 15–30, doi:10.1016/j.marchem.2013.04.006, 2013.

810 Radic, A., Lacan, F. and Murray, J. W.: Iron isotopes in the seawater of the equatorial Pacific Ocean: New
811 constraints for the oceanic iron cycle, Earth Planet. Sci. Lett., 306(1–2), 1–10, doi:10.1016/j.epsl.2011.03.015,
812 2011.

813 Raiswell, R., Benning, L. G., Tranter, M. and Tulaczyk, S.: Bioavailable iron in the Southern Ocean: The
814 significance of the iceberg conveyor belt, *Geochem. Trans.*, 9(1), 7, doi:10.1186/1467-4866-9-7, 2008.

815 Rijkenberg, M. J. A., Middag, R., Laan, P., Gerringa, L. J. A., Van Aken, H. M., Schoemann, V., De Jong, J. T.
816 M. and De Baar, H. J. W.: The distribution of dissolved iron in the West Atlantic Ocean, *PLoS One*, 9(6), 1–14,
817 doi:10.1371/journal.pone.0101323, 2014.

818 Sanders, R., Henson, S. A., Koski, M., De La Rocha, C. L., Painter, S. C., Poulton, A. J., Riley, J., Salihoglu, B.,
819 Visser, A., Yool, A., Bellerby, R. and Martin, A. P.: The Biological Carbon Pump in the North Atlantic, *Prog.*
820 *Oceanogr.*, 129(PB), 200–218, doi:10.1016/j.pocean.2014.05.005, 2014.

821 Sarthou, G., Lherminier, and the GEOVIDE team: Introduction to the French GEOTRACES North Atlantic
822 Transect (GA01): GEOVIDE cruise, *Biogeosciences*, 15, 7097-7109, <https://doi.org/10.5194/bg-15-7097-2018>,
823 2018.

824 Sarthou, G., Vincent, D., Christaki, U., Obernosterer, I., Timmermans, K. R. and Brussaard, C. P. D.: The fate of
825 biogenic iron during a phytoplankton bloom induced by natural fertilisation: Impact of copepod grazing, *Deep.*
826 *Res. Part II Top. Stud. Oceanogr.*, 55(5–7), 734–751, doi:10.1016/j.dsr2.2007.12.033, 2008.

827 Schlosser, C., Schmidt, K., Aquilina, A., Homoky, W. B., Castrillejo, M., Mills, R. A., Patey, M. D., Fielding, S.,
828 Atkinson, A. and Achterberg, E. P.: Mechanisms of dissolved and labile particulate iron supply to shelf waters
829 and phytoplankton blooms off South Georgia, Southern Ocean, *Biogeosciences*, 15, 4973–4993, doi: 10.5194/bg-
830 15-4973-2018, 2018.

831 Shelley, R. U., Landing, W. M., Ussher, S. J., Planquett, H. and Sarthou, G.: Characterisation of aerosol
832 provenance from the fractional solubility of Fe (Al, Ti, Mn, Co, Ni, Cu, Zn, Cd and Pb) in North Atlantic aerosols
833 (GEOTRACES GA01 and GA03), *Biogeosciences*, 15, 2271–2288, doi: 10.5194/bg-15-2271-2018, 2018

834 Shelley, R. U., Landing, W. M., Ussher, S. J., Planquette, H. and Sarthou, G.: Regional trends in the fractional
835 solubility of Fe and other metals from North Atlantic aerosols (GEOTRACES cruises GA01 and GA03) following
836 a two-stage leach, *Biogeosciences*, 15(1), 2271–2288, doi:10.5194/bg-15-2271-2018, 2018.

837 Sherrell, R. M., Field, P. M. and Gao, Y.: Temporal variability of suspended mass and composition in the
838 Northeast Pacific water column: Relationships to sinking flux and lateral advection, *Deep. Res. Part II Top. Stud.*
839 *Oceanogr.*, 45(4–5), 733–761, doi:10.1016/S0967-0645(97)00100-8, 1998.

840 Spinrad, R. W., Zaneveld, J. R. and Kitchen, J.C.: A Study of the Optical Characteristics of the Suspended Particles
841 Benthic Nepheloid Layer of the Scotian Rise, *J. Geophys. Res.*, 88, 7641–7645, doi:10.1029/83J003C, 1983.

842 Statham, P. J., Skidmore, M. and Tranter, M.: Inputs of glacially derived dissolved and colloidal iron to the coastal
843 ocean and implications for primary productivity, *Global Biogeochem. Cycles*, 22(3), 1–11,
844 doi:10.1029/2007GB003106, 2008.

845 Straneo, F., Pickart, R. S. and Lavender, K.: Spreading of Labrador sea water: An advective-diffusive study based
846 on Lagrangian data, *Deep. Res. Part I Oceanogr. Res. Pap.*, 50(6), 701–719, doi:10.1016/S0967-0637(03)00057-
847 8, 2003.

848 Sunda, W. G. and Huntsman, S. A.: Effect of Competitive Interactions Between Manganese and Copper on
849 Cellular Manganese and Growth in Estuarine and Oceanic Species of the Diatom *Thalassiosira*, *Limnol.*
850 *Oceanogr.*, 28(5), 924–934, doi:10.4319/lo.1983.28.5.0924, 1983.

851 Tagliabue, A., Bopp, L., Dutay, J. C., Bowie, A. R., Chever, F., Jean-Baptiste, P., Bucciarelli, E., Lannuzel, D.,
852 Remenyi, T., Sarthou, G., Aumont, O., Gehlen, M. and Jeandel, C.: Hydrothermal contribution to the oceanic
853 dissolved iron inventory, *Nat. Geosci.*, 3(4), 252–256, doi:10.1038/ngeo818, 2010.

854 Tagliabue, A., Bowie, A. R., Boyd, P. W., Buck, K. N., Johnson, K. S. and Saito, M. A.: The integral role of iron
855 in ocean biogeochemistry, *Nature*, 543(7643), 51–59, doi:10.1038/nature21058, 2017.

856 Taylor, S. and McLennan, S.: The geochemical evolution of the continental crust, *Rev. Geophys.*, 33(2), 241–
857 265, doi:10.1029/95RG00262, 1995.

858 Tebo, B. M. and Emerson, S. R.: Effect of Oxygen Tension Manganese (II) Concentration and Temperature on
859 the Microbially Catalyzed Manganese-II Oxidation Rate in a Marine Fjord, *Appl. Environ. Microbiol.*, 50(5),
860 1268–1273, 1985.

861 Tebo, B. M., Neelson, K. H., Emerson, S. and Jacobs, L.: Microbial mediation of Mn(II) and Co(II) precipitation
862 at the $\text{o}_2/\text{H}_2\text{S}$ interfaces in two anoxic fjords, 29(6), 1247–1258, 1984.

863 Tonnard, M., Planquette, H., Bowie, A. R., van der Merwe, P., Gallinari, M., Desprez de Gésincourt, F., Germain,
864 Y., Gourain, A., Benetti, M., Reverdin, G., Tréguer, P., Boutorh, J., Cheize, M., Menzel Barraqueta, J.L., Pereira-
865 Contreira, L., Shelley, R., Lherminier, P., and Sarthou, G.: Dissolved iron in the North Atlantic Ocean and
866 Labrador Sea along the GEOVIDE section (GEOTRACES section GA01), *Biogeosciences Discuss.*,
867 <https://doi.org/10.5194/bg-2018-147>, 2018

868 Trefry, J. H., Trocine, R. P., Klinkhammer, G. P. and Rona, P. A.: Iron and copper enrichment of suspended
869 particles in dispersed hydrothermal plumes along the mid-Atlantic Ridge, *Geophys. Res. Lett.*, 12(8), 506–509,
870 doi:10.1029/GL012i008p00506, 1985.

871 Ussher, S. J., Achterberg, E. P. and Worsfold, P. J.: Marine biogeochemistry of iron, *Environ. Chem.*, 1(2), 67–
872 80, doi:10.1071/EN04053, 2004.

873 Ussher, S. J., Worsfold, P. J., Achterberg, E. P., Laës, A., Blain, S., Laan, P., de Baar, H. J. W.: Distribution and
874 redox speciation of dissolved iron on the European continental margin, *Limnol. Oceanogr.*, 52(6), 2530–2539,
875 doi:10.4319/lo.2007.52.6.2530, 2007.

876 Van der Merwe, P., Lannuzel, D., Bowie, A. R., Mancuso Nichols, C. A. and Meiners, K. M.: Iron fractionation
877 in pack and fast ice in East Antarctica: Temporal decoupling between the release of dissolved and particulate iron

878 during spring melt, *Deep. Res. Part II Top. Stud. Oceanogr.*, 58(9–10), 1222–1236,
879 doi:10.1016/j.dsr2.2010.10.036, 2011a.

880 Van Der Merwe, P., Lannuzel, D., Bowie, A. R. and Meiners, K. M.: High temporal resolution observations of
881 spring fast ice melt and seawater iron enrichment in East Antarctica, *J. Geophys. Res. Biogeosciences*, 116(3), 1–
882 18, doi:10.1029/2010JG001628, 2011b.

883 Weinstein, S. E. and Moran, S. B.: Distribution of size-fractionated particulate trace metals collected by bottles
884 and in-situ pumps in the Gulf of Maine-Scotian Shelf and Labrador Sea, *Mar. Chem.*, 87(3–4), 121–135,
885 doi:10.1016/j.marchem.2004.02.004, 2004.

886 Yashayaev, I.: Hydrographic changes in the Labrador Sea, 1960-2005, *Prog. Oceanogr.*, 73(3–4), 242–276,
887 doi:10.1016/j.pocean.2007.04.015, 2007.

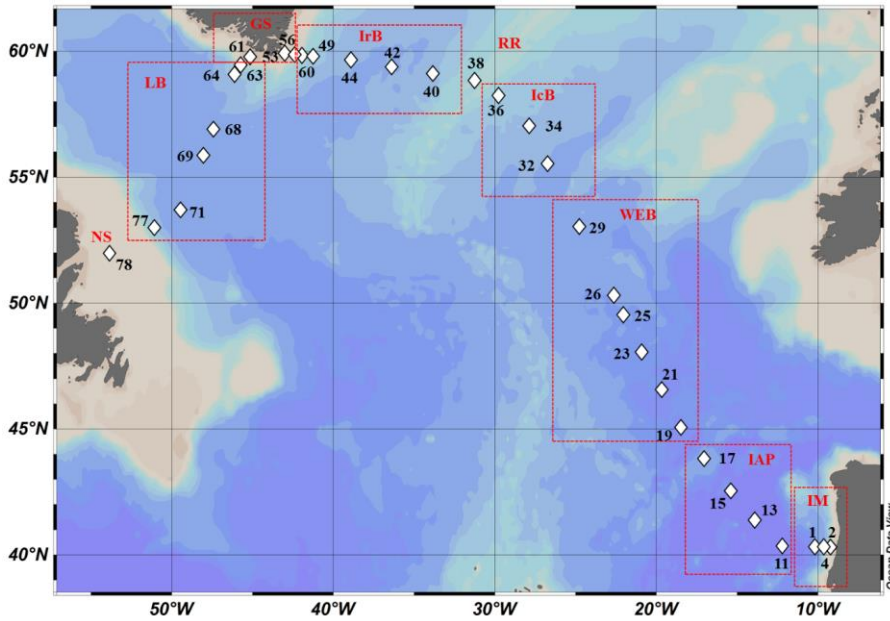
888 Yashayaev, I. and Loder, J. W.: Enhanced production of Labrador Sea Water in 2008, *Geophys. Res. Lett.*, 36(1),
889 doi:10.1029/2008GL036162, 2009.

890 Zunino, P., Lherminier, P., Mercier, H., Daniault, N., García-Ibáñez, M. I., and Pérez, F. F.: The GEOVIDE
891 cruise in May–June 2014 reveals an intense Meridional Overturning Circulation over a cold and fresh subpolar
892 North Atlantic. *Biogeosciences*, 14(23), 5323, 2017.

893
894
895
896
897
898
899
900
901
902
903
904
905
906
907
908
909
910
911
912
913
914

915
916
917
918
919
920
921
922
923
924
925
926

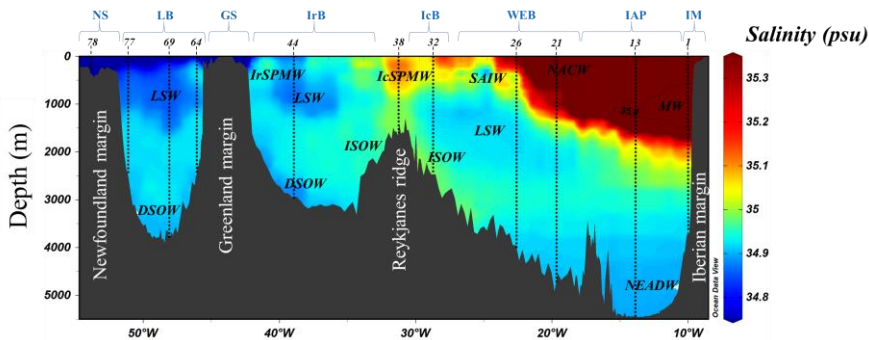
927 Figure 1: Map of stations where suspended particle samples were collected with GO-FLO bottles during the GEOVIDE
928 cruise (GA01) in the North Atlantic Ocean. Biogeochemical provinces are indicated by red squares, IM: Iberian
929 Margin, IAP: Iberian Abyssal Plain, WEB: Western European Basin, IcB: Iceland Basin, RR: Reykjanes Ridge, IrB:
930 Irminger Basin, GS: Greenland Shelf, LB: Labrador Basin, NS: Newfoundland Shelf. This figure was generated using
931 Ocean Data View (Schlitzer, R., Ocean Data View, odv.awi.de, 2017).



932
933
934
935
936
937

938
 939
 940
 941
 942
 943
 944
 945
 946
 947
 948
 949
 950
 951
 952
 953
 954
 955
 956

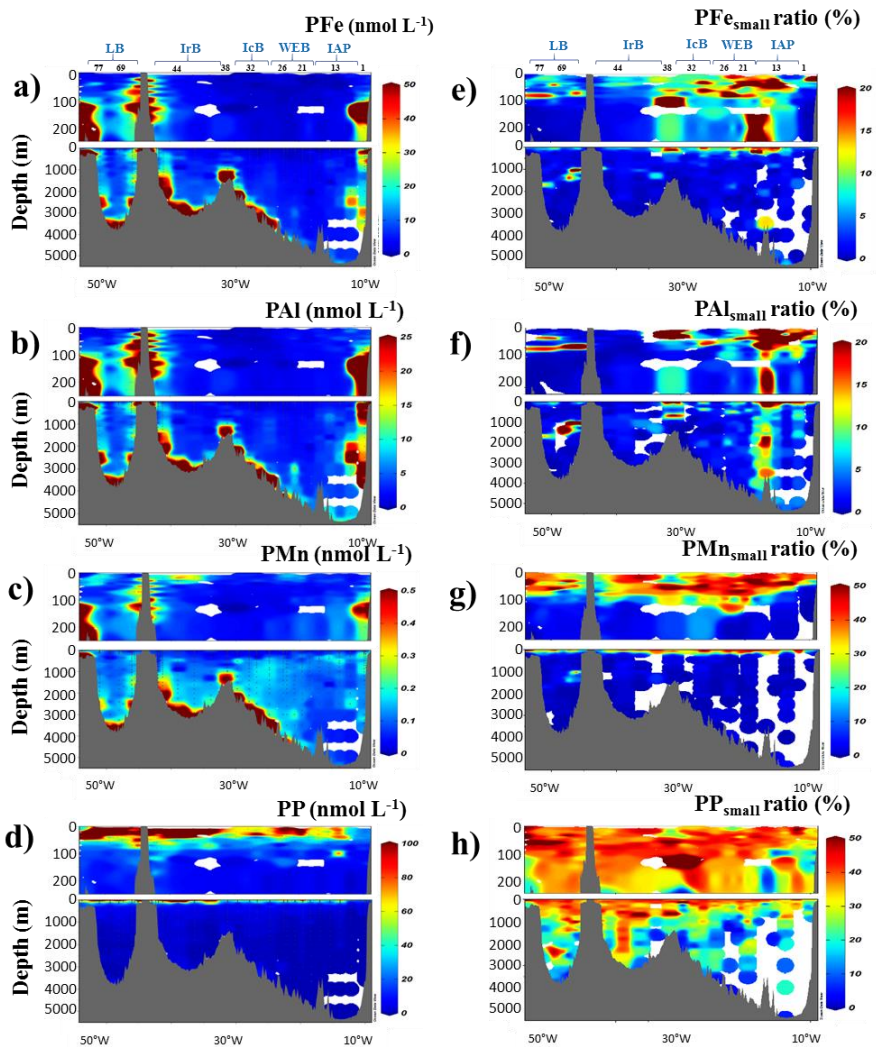
Figure 2: Salinity section during the GEOVIDE cruise with water masses indicated in black italic font. A salinity contour of 35.8 psu have been applied to identify the Mediterranean Water (MW) to the east. From right to left; North East Atlantic Deep Water (NEADW); North Atlantic Central Water (NACW); Labrador Sea Water (LSW); Sub-Arctic Intermediate Water (SAIW); Iceland-Scotland Overflow Water (ISOW); Iceland Sub-Polar Mode Water (IcSPMW); Denmark Strait Overflow Water (DSOW); Irminger Sub-Polar Mode Water (IrSPMW). Station locations are indicated by the numbers above the section and biogeochemical provinces are indicated in blue font above station numbers. This figure was generated using Ocean Data View (Schlitzer, R., Ocean Data View, odv.awi.de, 2017).



957
 958
 959
 960
 961
 962
 963
 964
 965
 966
 967

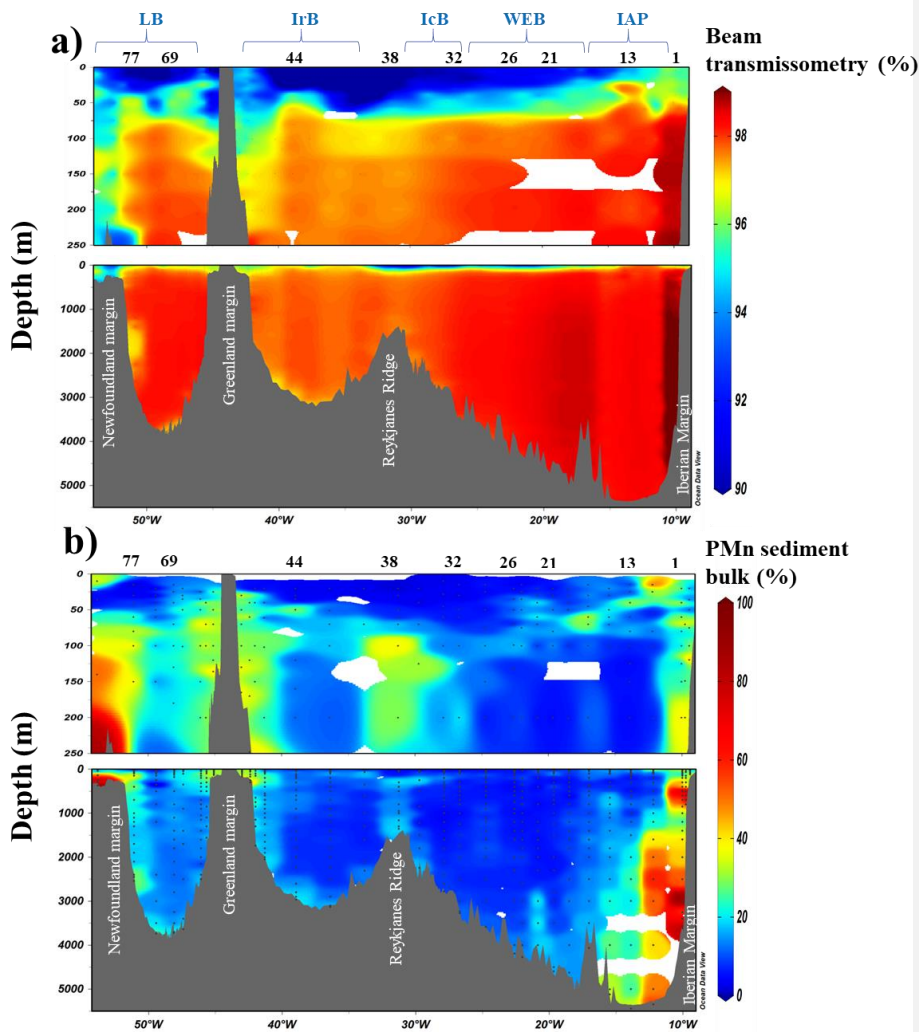
968
969
970
971
972
973
974
975
976
977

978 **Figure 3: Left panel: Distribution of total particulate (a) iron (PFe), (b) aluminium (PAI), (c) manganese (PMn) and**
979 **(d) phosphorus (PP) concentrations (nmol L⁻¹) in the first 250 m and the entire water column along the GEOVIDE**
980 **section in the North Atlantic Ocean. Right panel: Contribution of the small size fraction (0.45-5 µm) expressed as a**
981 **percentage (%) of the total concentration of (e) PFe, (f) PAI, (g) PMn and (h) PP. Station IDs and biogeochemical**
982 **regions are indicated on top of sections a and e. This figure was generated using Ocean Data View (Schlitzer, R., Ocean**
983 **Data View, odv.awi.de, 2017).**



984
 985
 986
 987
 988
 989
 990
 991

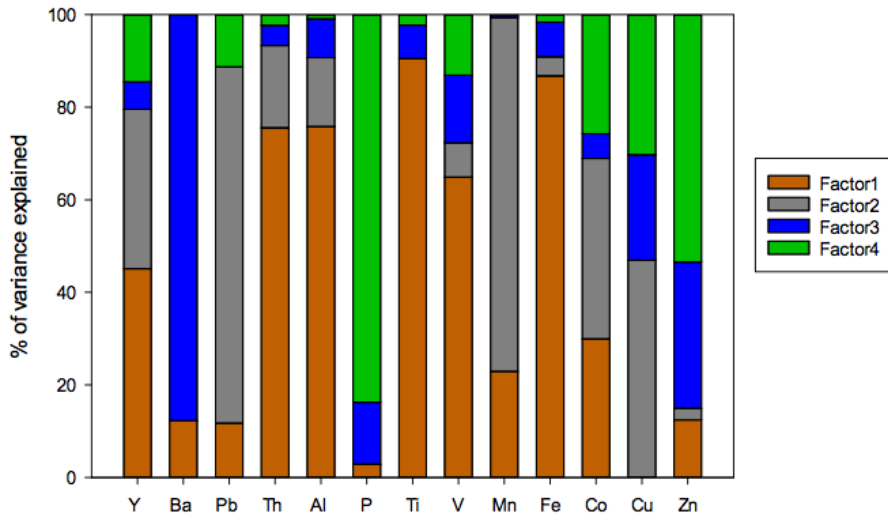
Figure 4: Section of derived contributions of sedimentary inputs along the GA01 section with (a) beam transmissometry (%) and (b) manganese bulk sediment proxy (%) based on Eq (3). Station IDs and biogeochemical region are indicated above section (a) in black numbers and blue letters, respectively. This figure was generated using Ocean Data View (Schlitzer, R., Ocean Data View, odv.awi.de, 2017).



992
 993
 994
 995
 996
 997
 998
 999
 1000

Figure 5: Factor fingerprint of the positive matrix factorisation conducted on 445 particles samples collected along the GA01 section. The four main factors influencing the particulate trace element variance are represented in a stacked bar chart of the percentage of variance explained per element. Factor 1 is dominated by the lithogenic elements, e.g.

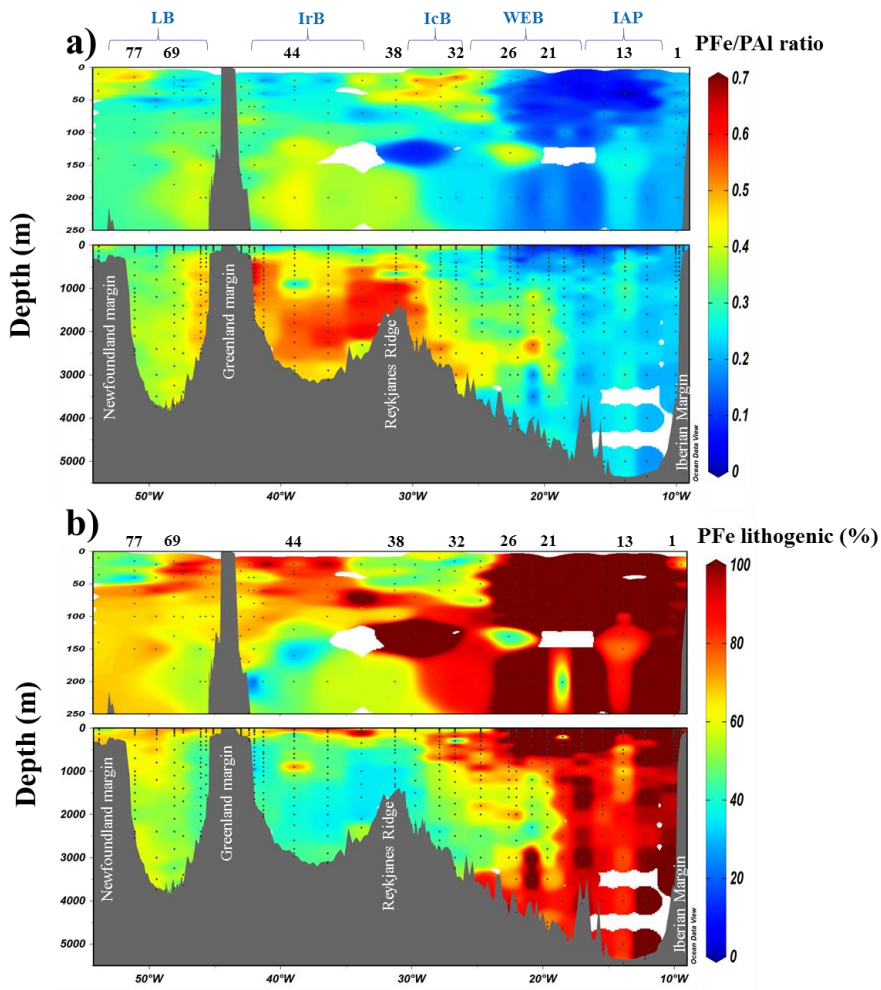
1001 Th, Al, Ti and Fe. Factor 2 is associated with Pb and Mn variances. Biogenic barite formation mainly influences factor
1002 3. Factor 4 is dominated by biogenic elements, e.g. P, Co, Cu and Zn.



1003
1004
1005
1006
1007
1008
1009
1010
1011
1012
1013
1014
1015
1016
1017
1018
1019
1020

1021
1022
1023
1024

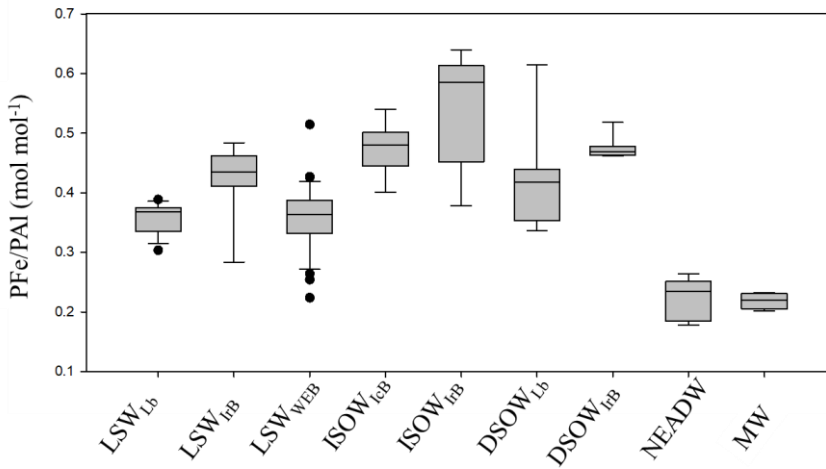
Figure 6: a) Section of the PFe to PAI molar ratio (mol mol^{-1}) during the GEOVIDE cruise (GA01) and (b) contribution (%) of lithogenic particulate iron ($\text{PFe}_{\text{litho}}$) based on Eq. (1). Station IDs and biogeochemical provinces are indicated above each section in black numbers and blue letters, respectively. This figure was generated using Ocean Data View (Schlitzer, R., Ocean Data View, odv.awi.de, 2017).



1025
1026
1027
1028
1029
1030

1031
1032
1033
1034
1035
1036
1037
1038
1039
1040

Figure 7: Box and whisker diagram of PFe/PAI molar ratio in nine water masses sampled along the GA01 section in the North Atlantic Ocean. Water masses are defined in section 3.1 and in Figure 2. The PFe/PAI median values for each water masses with the biogeochemical provinces in subscript were as follows: $LSW_{LB} = 0.37$; $LSW_{LFB} = 0.44$; $LSW_{WEB} = 0.36$; $ISOW_{LFB} = 0.48$; $ISOW_{LFB} = 0.58$; $DSOW_{LFB} = 0.42$; $DSOW_{LFB} = 0.47$; $NEADW_{LAP} = 0.23$; $MW = 0.22 \text{ mol mol}^{-1}$. The difference in PFe/PAI between water masses is statistically significant (Kruskal-Wallis test; $p < 0.001$ excluding water masses for which we had less than 5 data points for PFe/PAI). Noted that the UCC PFe/PAI ratio reported from Taylor and McLennan, (1995) is $0.21 \text{ mol mol}^{-1}$.



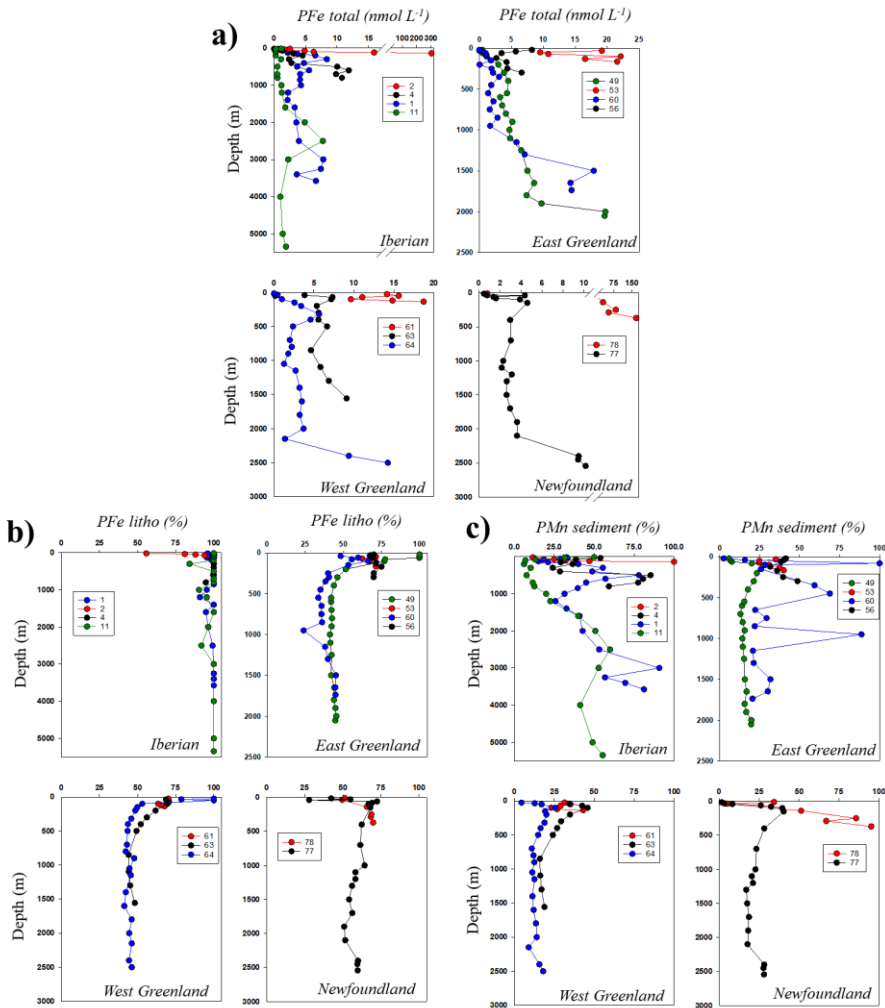
1041
1042
1043
1044
1045
1046
1047
1048
1049
1050
1051
1052
1053
1054
1055

Formatted: Font: (Default) Calibri, 11 pt

Formatted: Body, Left

1056
1057

1058 **Figure 8:** Vertical profiles of (a) PFe (nmol L⁻¹), (b) lithogenic proportion of particulate iron (PFe_{litho}, %) and (c)
1059 sedimentary proportion of particulate manganese (PMn sediment, %) at the Iberian, East-West Greenland and
1060 Newfoundland margins.



1061

1062

1063

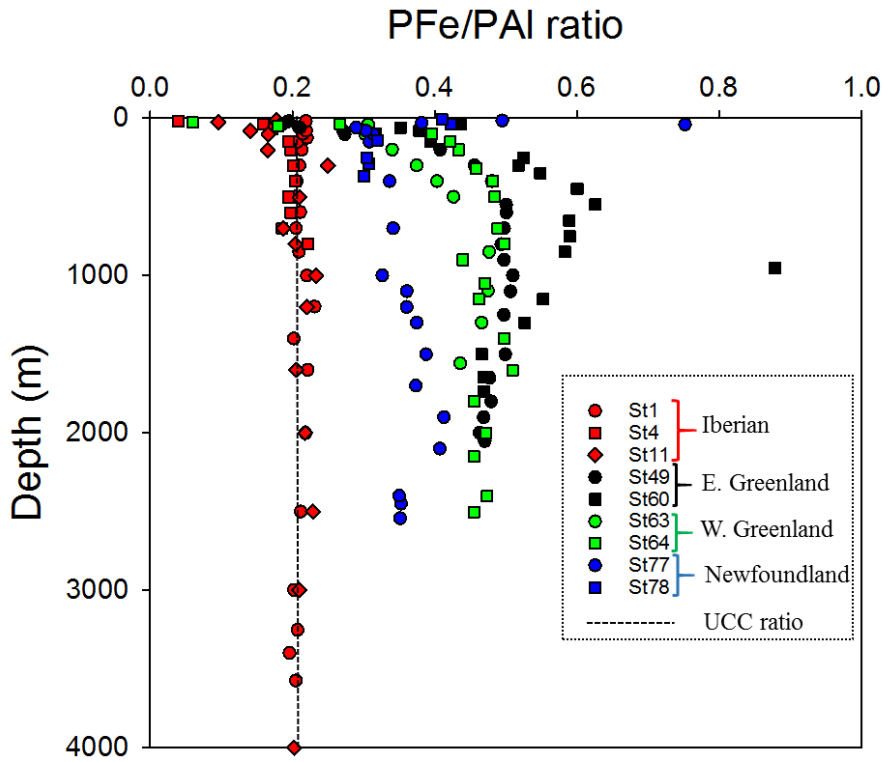
1064

1065

1066

1067

1068 Figure 9: Scatter of the PFe/PAI ratio at the Iberian (red dots), East Greenland (black dots), West Greenland (green
1069 dots) and Newfoundland margins (blue dots). Dashed line indicate the UCC PFe/PAI ratio (Taylor and McLennan,
1070 1995).



1071

1072

1073

1074

1075

1076

1077

1078

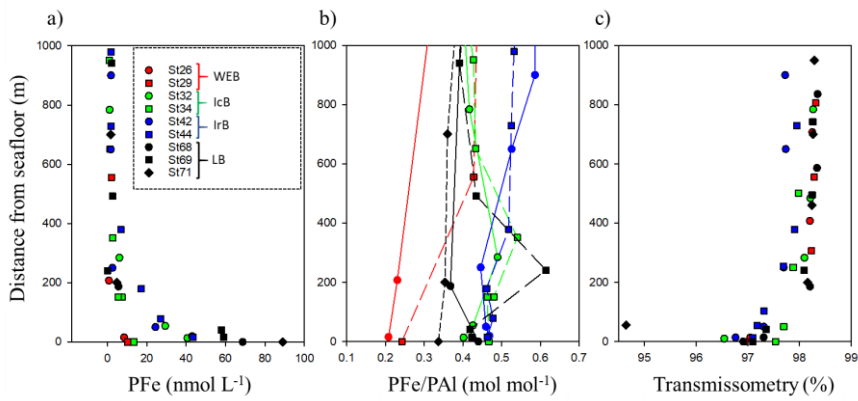
1079

1080

1081

1082 **Figure 10: Benthic Nepheloid Layers (BNLs) encountered along the GA01 section and observed through a) PFe total;**
1083 **b) PFe/PAI ratio and c) beam transmissometry (%) as a function of depth above the seafloor (m) at selected stations**
1084 **where a decrease in transmissometry was recorded in the West European (red dots), the Iceland (green dots), the**
1085 **Irminger (blue dots) and the Labrador Basins. Noted that the UCC PFe/PAI ratio reported from Taylor and McLennan,**
1086 **(1995) is 0.21 mol mol⁻¹.**

1087



1088

1089

1090

1091

1092

1093

1094

1095

1096

1097

1098

1099

1100

1101

1102

1103

		Fe	Al	P	Mn
Blank (nmol L ⁻¹)	5µm filter	0.072	0.100	0.511	0.003
	0.45µm filter	0.132	0.164	1.454	0.005
Limit of detection (nmol L ⁻¹)	5µm filter	0.011	0.030	0.365	0.001
	0.45µm filter	0.026	0.046	1.190	0.001
Recovery CRM (%)	BCR-414 (n=10)	88 ± 7			94 ± 7
	MESS-4 (n=5)	98 ± 14	97 ± 14	80 ± 30	110 ± 18
	PACS-3 (n=8)	101 ± 9	99 ± 14	91 ± 34	112 ± 11

1104

1105 **Table 1: Blank and limit of detection (nmol L⁻¹) of the two filters and certified reference material (CRM)**
 1106 **recoveries during GEOVIDE suspended particle digestions.**

1107

1108

1109

1110

1111

1112

Location	Depth range	PFe	PAI	PMn	PP	Fraction	Author	Year
N. Atlantic (>40°N)	All	bdl-304	bdl-1544	bdl-3.5	bdl-402	>0.45µm	This study	
Labrador Sea	0-250	0.1-1.2	0.1-1.5			>53 µm	Weinstein et al.	2004
Labrador Sea	0-250	2.5	3.6	0.05		0.4–10µm	Weinstein et al.	2004
N. Atlantic (25-60°N)	Upper 1000m	0.29-1.71	0.2-19.7			0.4µm	Barrett et al.	2012
N. Atlantic	All	0-938	0-3600			0.8–51 µm	Ohnemus et al.	2015
Gulf of Maine	0-300	34.8	109			>0.4 µm	Weinstein et al.	2004
Eastern tropical N.A.	0-200		0.59-17.7			>0.2 µm	Dammshausser et al.	2013
Eastern tropical N.A.	0-600	ND-12				1–51 µm	Lam et al.	2012
Sub-tropical N.A.	All	ND-140	ND-800			>0.45µm	Milne et al.	2017
Meridional Atlantic	0-200		0.35-16.1			>0.2 µm	Dammshausser et al.	2013
Northeast Pacific	0-3557		0.0-54.2			1-53µm	Sherrell et al.	1998
Eastern tropical S.Pacific	All	bdl-159	bdl-162	bdl-8.7	bdl-983	>0.8 µm	Lee et al.	2017
South Georgia Shelf	All	0.87-267	0.6-195	0.01-3.85		>1 µm	Schlosser et al.	2017
Southern Ocean	30-340	0.15–13.2	0.11–25.5			>53 µm	Planquette et al.	2009
East Antarctic	Surface		0.02-10.67	0.01-0.14		>0.2 µm	Lannuzel et al.	2011
East Antarctic	Fast ice	43-10385	121-31372	1-307		>0.2 µm	Lannuzel et al.	2014
Ross Sea	All	0.68-57.3	ND-185	ND-1.4	5.4-404	>0.4 µm	Marsay et al.	2017

1113

1114 **Table 2: Concentration (in nmol L⁻¹) of particulate trace elements (PFe, PAI, PMn and PP) in suspended**
 1115 **particles collected in diverse regions of the world's ocean. Bdl: below detection limit, ND: non-determined.**

1116

1117